# The hydrogen isotopic composition of lunar melt inclusions: An interplay of complex magmatic and secondary processes

Journal Item

Available online at www.sciencedirect.com

ScienceDirect

Geochimica et Cosmochimica Acta 284 (2020) 196–221

Geochimica et Cosmochimica Acta

www.elsevier.com/locate/gca

# The hydrogen isotopic composition of lunar melt inclusions: An interplay of complex magmatic and secondary processes

A. Stephant [a,*], M. Anand [a,b], R. Tartèse [c], X. Zhao [a], G. Degli-Alessandrini [a], I.A. Franchi [a]

[a] School of Physical Sciences, The Open University, Milton Keynes MK7 6AA, UK
[b] Department of Earth Sciences, The Natural History Museum, London SW7 5BD, UK
[c] Department of Earth and Environmental Sciences, The University of Manchester, Manchester M13 9PL, UK

Received 21 December 2019; accepted in revised form 18 June 2020; available online 29 June 2020

**Abstract**

Since the discovery of water (a term collectively used for the total H, OH and $H_2O$) in samples derived from the lunar interior, heterogeneity in both water concentration and its hydrogen isotopic ratio has been documented for various lunar phases. However, most previous studies have focused on measurements of hydrogen in apatite, which typically forms during the final stages of melt crystallisation. To better constrain the abundance and isotopic composition of water in the lunar interior, we have targeted melt inclusions (MIs), in mare basalts, that are trapped during the earliest stages of melt crystallisation. Melt inclusions are expected to have suffered minimal syn- or post-eruption modification processes, and, therefore, should provide more accurate information about the history of H in the lunar interior. Here, we report $H^-/^{18}O^-$ measurements as calibrated water concentrations, and hydrogen isotope ratios obtained by secondary ion mass spectrometry (SIMS) in a large set of basaltic MIs from Apollo mare basalts 10020, 10058, 12002, 12004, 12008, 12020, 12040, 14072 and 15016. Our results demonstrate that partially crystallised MIs from lunar basalts and their parental melts were influenced by a variety of processes such as hydrogen diffusion, degassing and assimilation of material affected by solar-wind implantation. Deconvolution of these processes show that lunar basaltic parental magmas were heterogeneous and had a broadly chondritic hydrogen isotopic composition with δD values varying between −200 and +200‰.


*Keywords:* Moon; Volatile; Hydrogen; Melt inclusion; NanoSIMSIshlinskii' theorem

## 1. INTRODUCTION

Since the discovery of indigenous water in lunar volcanic glasses (Saal et al., 2008), the abundance and origin of water in the lunar mantle has been vigorously debated (it is important to note that the term "water" used here collectively refers to all major forms of hydrogen (i.e., H, OH, $H_2O$), being measured in the target lunar mineral/phase). Estimates for the bulk-Moon $H_2O$ content (calculated as μg/g) based on measured ratios of moderately volatile elements (e.g., Zn/Fe) in lunar samples and volatilities of respective elements point to an anhydrous Moon (<1μg/g $H_2O$) (Albarede et al., 2015). On the other hand, measurements of water (H, OH, $H_2O$) abundances in lunar volcanic glasses (LVG) and olivine-hosted MIs (Saal et al., 2008; Hauri et al., 2011; Füri et al., 2014; Chen et al., 2015; Ni et al., 2019), plagioclase (Hui et al., 2013, 2017), and apatite (Boyce et al., 2010; McCubbin et al., 2010a, 2010b; Greenwood et al., 2011; Barnes et al., 2013, 2014; Tartèse et al., 2013, 2014; Boyce et al., 2015) indicate a $H_2O$-richer Moon, with estimates ranging from ~1 to ~450 μg/

* Corresponding author.
*E-mail address:* alice.stephant@open.ac.uk (A. Stephant).

https://doi.org/10.1016/j.gca.2020.06.017
0016-7037/

g $H_2O$ for at least some portions of the lunar mantle (McCubbin et al., 2010b; Hauri et al., 2011, 2015; Hui et al., 2013, 2017; Tartèse et al., 2013; Füri et al., 2014; Chen et al., 2015; Ni et al., 2019). This range of water content for the lunar mantle is still an order of magnitude lower than some estimates for the water content of the bulk silicate Earth (*ca.* 1000–3000 μg/g $H_2O$ (Marty, 2012); 1100 ± 220 μg/g $H_2O$ (Palme and O'Neil, 2014); 3900 $^{+32700}_{-3300}$ μg/g $H_2O$ (Peslier et al., 2017; and ref. therein)). Nevertheless, the upper end of the estimated range of water content for the lunar mantle is consistent with some estimates of the water content of the Earth's primitive mantle (*ca.* 300 ± 100 μg/g (Halliday, 2013); 268 ± 134 μg/g (Zhang, 2014)). Overall, Taylor (2014) states that it would seem unusual if the water content of the Moon were similar to that of Earth's mantle. It has also been suggested that water is heterogeneously distributed among the different lunar reservoirs (Anand, 2010; McCubbin et al., 2011; Robinson and Taylor, 2014), with source regions for mare basalt and pyroclastic volcanic samples being richer in water compared to the source regions for non-mare intrusive rocks (Barnes et al., 2014; Robinson et al., 2016).

As a result of the incompatible nature of H during crystallisation of major silicate minerals such as olivine, pyroxene, and plagioclase, $H_2O$ enrichment is expected in later formed products of the lunar magma ocean (LMO) crystallisation. The apparent discrepancy between the water contents of mare and non-mare rocks is thus at odds with non-mare materials being formed from late-stage LMO products. Differences in water abundance between mare and non-mare source regions may be linked to their respective ages of formation; the younger mare basalts and pyroclastic deposits having incorporated late-delivered components (Tartèse and Anand, 2013; Barnes et al., 2016). Another possible explanation for the discrepancy between the water contents of mare and non-mare material may be related to degassing of $H_2O$ towards the end of the LMO crystallisation leaving late-stage LMO products depleted in $H_2O$ (Hui et al., 2017). Among basaltic and volcanic products, the higher water concentration of the high-Ti 74220 primitive melt, calculated from diffusion modelling of volcanic glasses (Saal et al., 2008) and recorded in their MIs (Hauri et al., 2011), has been used to calculate a water content for their mantle source region of ~100 to 300 μg/g $H_2O$. This sample has been considered an anomaly, and, thus not a representative of the lunar interior, implying local heterogeneities in the lunar mantle (Albarede et al., 2015). However, recent work on MIs from Apollo 11, Apollo 12, and Apollo 15 mare basalt suites are consistent with a lunar mantle with a water content of ~80–100 μg/g (Chen et al., 2015; Ni et al., 2019).

The primordial hydrogen isotopic composition of indigenous lunar water has been inferred to be between ~−300 and +300‰ (the H isotopic composition is reported using the δD notation, which represents the deviation from the H isotope composition of terrestrial oceans in part per thousand, following $\delta D = [(D/H_{sample})/(D/H_{VSMOW})\text{-}1] \times 1000$, where $D/H_{VSMOW} = 155.76 \times 10^{-6}$; Hagemann et al., 1970; Gonfiantini, 1978). Hydrogen isotope measurements on lunar volcanic glasses suggest an initial source with a δD value between + 187 ± 19‰ and + 274 ± 42‰ (Saal et al., 2013; Füri et al., 2017 and ref. therein). Apatite from mare basalt generally have δD values > +500‰ (Barnes et al., 2013; Tartèse et al., 2013), which have been interpreted as resulting from the fractionation of D/H ratios in late-stage basaltic melts after extensive $H_2$ degassing from an initial H isotope composition similar to carbonaceous chondrites. Apatite from non-mare materials such as the Mg-suite and alkali-suite display lower average δD values of −281 ± 49‰ (Barnes et al., 2014). In case of evolved-rocks such as quartz monzodiorites (QMDs), from the Apollo 15 collection, apatite record some of the lowest δD values ever reported for lunar samples (−754 ± 57‰; Robinson et al., 2016), suggesting that H isotopes in their magmas were not fractionated by $H_2$ degassing, and that there may exist some local heterogeneities in terms of water reservoirs in the lunar interior (Robinson and Taylor, 2014; Robinson et al., 2016). The whole picture is complicated by the fact that magmatic and secondary processes such as degassing, spallation reaction producing D, and/or incorporation of regolith, enriched in solar wind H (Stephant and Robert, 2014; Treiman et al., 2016; Singer et al., 2017), as well as speciation of H in lunar melts (Elkins-Tanton and Grove, 2011; Renggli et al., 2017) can all potentially induce δD variations among lunar samples, and could be, in part, responsible for the apparent δD heterogeneity observed among various lunar reservoirs. For instance, Hui et al. (2017) recently proposed that heterogeneous δD values among different lunar reservoirs could result from degassing of the LMO, with the deeper and undegassed lunar interior being characterised by a δD value of ~−281 ± 49‰, as recorded by apatite in Mg-suite norites (Barnes et al., 2014), and a degassed interior reservoir characterised by δD values around +310 ± 110‰, as measured in plagioclase from ferroan anorthosite 60015 (Hui et al., 2017). Desch and Robinson (2019) proposed an alternative hypothesis to explain the heterogeneity in δD among different lunar reservoirs by suggesting that the Moon-forming impactor Theia, carried a nebular H isotope signature (i.e., −865‰; (Geiss and Gloecker, 1998)), which might be reflected in the very low-δD values measured in some of Apollo 15 QMDs (−754 ± 57‰; Robinson et al., 2016).

Among the variety of lunar phases studied so far, MIs are potentially the ideal candidates for unravelling the abundance and H isotopic composition of primordial lunar water. Melt inclusions are small droplets of silicate melts trapped during phenocryst growth at magmatic pressures and temperatures, which theoretically shield them from subsequent degassing or crystal fractionation effects during the eruption and emplacement of a magma (Walker et al., 1976; Roedder, 1979; Lowenstern, 2003; Métrich et al., 2008; Moore et al, 2015; Cannatelli et al., 2016). As such, MIs supposedly record the volatile composition of the magma (such as $H_2O$, Cl, $CO_2$, S, F) at the time of melt entrapment.

The speciation of hydrogen in amorphous silicates such as melt inclusions can occur in different forms (e.g., H, $H_2$, OH, $H_2O$, $CH_4$, $H_2S$, $NH_3$) depending on parameters such as pressure, temperature, melt composition, the concentra-

tions of other volatiles (C, N, F, Cl, S), water and oxygen fugacities (Holloway and Blank, 1994; Elkins-Tanton and Grove, 2011; Peslier et al., 2017; Renggli et al., 2017; Dalou et al., 2019; Grewal et al., 2020). In fact, $H_2O$ can be dissolved as $OH^-$ with decreasing temperature of the melt (Nowak and Behrens, 1995). Given the oxygen fugacity of lunar samples, Elkins-Tanton and Grove (2011) stated that atomic H will be as abundant as $H_2O$ in lunar melt phases, while Renggli et al. (2017) found that $H_2$ is the most abundance hydrogen species in lunar gas. Grewal et al. (2020) stated that while much of H would be present in N-H or C-H bearing species, H would also be present in the form of OH in the silicate melt if the bulk H content of the silicate melt is much higher than the bulk N content. It is important to note that for SIMS measurements, it is not possible to confirm the speciation of hydrogen. As such, even though hydrogen might be distributed among different species in the lunar melt, throughout this paper, we have chosen to report $H^-/^{18}O^-$ measured in lunar MIs as $H_2O$ or water.

A major challenge in using MIs for inferring the volatile composition of a melt, and especially hydrogen, is that some magmatic and secondary processes can alter both the $H_2O$ content and δD value of a MI after entrapment. This, issue can be further compounded by the hydrogen speciation, that could also induce some isotopic fractionation. Indeed, $H_2O$ loss (i.e., shallow level degassing; Hauri, 2002), $H^+$ diffusion through the host (Hauri, 2002; Massare et al., 2002; Severs et al., 2007; Gaetani et al., 2012; Bucholz and Gaetani, 2013; Chen et al., 2013; Ni et al., 2017), as well as post-entrapment crystallisation (PEC) (Danyushevsky et al., 2002; Steele-MacInnis et al., 2011) could alter the original water budget and hydrogen isotopic signature. However, because these processes affect both $H_2O$ and δD, they produce systematic variations that can be identified using a coupled $H_2O$-δD dataset for MIs.

Despite many challenges, water concentrations in MIs have been used for investigating $H_2O$ abundances in planetary bodies such as the Earth (e.g., Esposito et al., 2012; Hauri, 2002; Wallace, 2005), Mars (e.g., Giesting et al., 2015; Usui et al., 2012) and the Moon (e.g., Chen et al., 2015; Saal et al., 2013; Hauri et al., 2011; Singer et al., 2017; Ni et al., 2019; Greenwood et al., 2019). Lunar basalts from Apollo 11 and Apollo 12 are known to contain abundant MIs, as first demonstrated in the pioneering work of Roedder and Weiblen (1970, 1971). However, the first analysis of water concentration and δD in lunar MIs was achieved only recently, in sample 74220 (Hauri et al., 2011; Saal et al., 2013). Results indicated an initial $H_2O$ content of ~100 to 300 μg/g (Hauri et al., 2015) for the lunar mantle, associated with a δD value of $+187 \pm 19$‰ (Saal et al., 2013). Results from these MIs are comparable to those obtained on volcanic glasses in sample 74002 for which a δD value of $+274 \pm 42$‰ was reported by Füri et al. (2017). Based on $H_2O$/Ce ratios measured in MIs from various mare basalts, water concentrations of around ~ 80–100 μg/g have been estimated for their lunar mantle source regions (Chen et al., 2015; Ni et al., 2019), which are consistent with estimated water concentrations in the mantle source regions of pyroclastic glasses. So far only two studies have reported the D/H ratio of water in MIs in mare basalts (Apollo 12 basaltic suite; Singer et al., 2017; Greenwood et al., 2019). These studies reported a range of δD values ($-183 \pm 212$‰ to $+138 \pm 61$‰) all of which were lower than δD values recorded in pyroclastic glasses and their MIs (note that these values are not corrected for spallation-produced D and, therefore, should be viewed as an upper limit). These lower δD values in mare basalt MIs were interpreted in terms of an exchange of deuterium and hydrogen with the lunar regolith during cooling of the Apollo 12 olivine basalts (Singer et al., 2017; Greenwood et al., 2019).

To develop a comprehensive understanding of D/H ratios in MIs from mare basalts, and to provide more robust constraints on the D/H ratio(s) of water in mare-basalt source regions, we have analysed the H concentration and its associated H isotopic composition in olivine- and pyroxene-hosted MIs from nine different samples from four Apollo missions. We converted the $H^-/^{18}O^-$ ratio measured into equivalent $H_2O$ concentration, as stated previously. These data are then used to constrain the abundance and source of H in their respective parent-melt and investigate any variations among respective volatile reservoirs. We have also analysed water abundance and isotopic composition in apatite from the same samples where literature data were not available in order to investigate the relationship between water abundance and D/H ratio between earlier-formed MIs and later-formed apatite in a given sample.

## 2. MATERIALS AND METHODS

### 2.1. Standards

Several terrestrial standards were used for water abundance calibrations and instrumental mass fractionation (IMF) corrections of data acquired on MIs and apatite. The first set of standards, used for MI analyses, includes: San Carlos olivine, which was used effectively as a dry standard for background monitoring; terrestrial basaltic glasses from the Southwest Indian Ridge DR5, DR15 and DR20 for IMF correction and for $H_2O$ calibration. These standards were mounted in 10 mm diameter aluminium mounts filled with indium, following the protocol established in previous studies (Aubaud et al., 2007; Mosenfelder et al., 2011). As was done previously in several studies of hydrogen in nominally anhydrous minerals (NAMs) (Aubaud et al., 2007; Hauri et al., 2002; Koga et al., 2003; Mosenfelder et al., 2011; Tenner et al., 2009), these standards were baked overnight at 115 °C before being pressed into an indium mount. The second set of standards for phosphate analyses includes San Carlos olivine, for background monitoring, and apatites Ap003, Ap004 and Ap018 (McCubbin et al., 2012). These standards were also mounted in indium, in the same manner as the first set. Both sets of standards were baked in an oven at ~50 °C overnight for ~17 h before being gold-coated and introduced into the NanoSIMS. The chemical composition, $H_2O$ concentrations and δD values of the terrestrial standards are provided in supplementary Table S1.

### 2.2. Samples

Forty-two olivine-hosted MIs and fourteen pyroxene-hosted MIs were selected from nine polished thin sections of Apollo basalt samples 10020,31; 10058,254; 12002,562; 12004,51; 12008,18; 12020,8; 12040,44; 14072,13 and 15016,14; prepared at NASA Johnson Space Center using a water-free medium. A selection of backscattered electron (BSE) images are presented in Fig. 1 (a larger set of BSE images can be found in supplementary Fig. S1). The samples were selected based on the probability of finding MIs. Samples from the Apollo 12 collection were thus selected since they have been extensively studied previously for MIs (Roedder and Weiblen, 1971; Bombardieri et al., 2005; Chen et al., 2015; Singer et al., 2017). Samples from other Apollo landing sites (i.e., Apollo 11, 14, 15) were also selected to expand the spatial coverage of the sample set and explore any potential variations among their hydrogen abundance and isotopic composition. For inter-laboratory comparisons, a few samples in which MIs were analysed in previous studies were also selected (Chen et al., 2015; Ni et al., 2017; Singer et al., 2017).

Samples 10020 and 10058 are high-Ti/low-K basalts (Fig. 2), with 10020 having a fine-grained texture and 10058 having a coarser-grained texture. Their cosmic ray exposure (CRE) ages are 130 Ma and 70 Ma, respectively (Guggisberg et al., 1979). In 10020, the presence of MIs in olivine phenocrysts has been documented in the literature (Meyer, 2009). In contrast, olivine is rare in 10058 (Beaty and Albee, 1978), and therefore only pyroxene-hosted MIs could be studied. The $H_2O$ content and δD values of some apatite grains in 10058 were reported previously by Tartèse et al. (2013).

Of the Apollo 12 suite, five samples have been investigated in this study: 12002, 12004, 12008, 12020, 12040. All of these basalts are low-Ti basalts (Fig. 2). The medium-grained porphyritic olivine basalt 12002 has a CRE age between 92 Ma (Bogard et al., 1971) and 161 ± 20 Ma (Alexander, 1971). The older CRE age was chosen for spallation correction because Füri et al. (2017) showed that CRE ages of most Apollo samples have likely been underestimated. The porphyritic olivine basalt 12004 has 40% of its mass represented by olivine and pyroxene phenocrysts (Meyer, 2009). Hintenberger et al. (1971) determined CRE ages for 12004 using $^{3}He$ (60 Ma), $^{21}Ne$ (53 Ma) and $^{38}Ar$ (45 Ma). It has been recalculated recently by Füri et al. (2017) with values spanning between 60 and 70 Ma; we selected an average exposure age of 66 ± 12 Ma. Basalt 12008 is composed of olivine phenocrysts surrounded by dendritic pyroxenes. The presence of circular olivine-hosted MIs has been reported in this sample (Meyer, 2009). Stettler et al. (1973) determined a $^{38}Ar$ exposure age of 50 Ma. Basalt 12020 is a medium-grained olivine microgabbro (Klein et al., 1971). Its $^{21}Ne$ exposure age was estimated first at 71 Ma (Hintenberger et al., 1971) and then recently re-estimated between 73 Ma and 111 Ma (Füri et al., 2017). We selected an average CRE age of 91 ± 15 Ma for this study. Low-Ti basalt 12040 is a slowly cooled olivine basalt (Walker et al., 1976) with a high proportion of mafic minerals. The widespread occurrence of MIs in olivine and pyroxene has been highlighted since the return of this sample (Newton et al., 1971). As such, H in MIs in 12040 has been studied before (Chen et al., 2015; Singer et al., 2017). However, basalt 12040 has a very old CRE age of ~285 ± 50 Ma (Burnett et al., 1975). Additionally, previous studies involving $H_2O$-δD systematics in apatite and MIs have raised the possibility that this sample may have incorporated solar wind hydrogen (Boyce et al., 2015; Treiman et al., 2016; Singer et al., 2017).

High-Al basalt 14072 is an olivine basalt with medium-sized olivine phenocrysts, also classified as a low-Ti basalt (Fig. 2). The Apollo 14 mission landed on the Fra Mauro Formation, which is part of the ejecta blanket that formed from the excavation of the Imbrium Basin at ~3.93 Ga (Nemchin et al., 2009; Snape et al., 2016). The $^{38}Ar$ exposure age of sample 14072 has been estimated to be 21 Ma (York et al., 1972).

Finally, 15016 is a medium-grained, vesicular, olivine-normative (Meyer, 2009) low-Ti basalt (Fig. 2). Similar to sample 12040, it is a slowly cooled basalt. The CRE age of 15016 has been re-evaluated recently by Füri et al. (2017) to be between 378 ± 66 and 422 ± 73 Ma. As such, we decided to use the average of ~400 ± 73 Ma for this study. The $H_2O$ abundances and δD values of apatite grains in 15016 have been reported previously (Barnes et al., 2019).

Almost all of the studied forty-two olivine-hosted MIs and fourteen pyroxene-hosted MIs are partially crystallised, with a few exceptions of "glassy" MIs (only four MIs have a post-entrapment crystallisation (PEC) percentage, i.e., the percentage of daughter minerals, <10%). While some previous workers have argued in favour of homogenisation experiments on MIs in order to ascertain the initial $H_2O$ abundances of their melts (Esposito et al., 2012; Chen et al., 2015), a recent study on MIs from Apollo 12 basalts has shown that $H_2O$ contents, measured in partially-crystallised MIs, do not exhibit significant variations compared to glassy ones (Singer et al., 2017; and references therein).

### 2.3. Scanning Electron Microscope and Electron Microprobe

Backscattered electron imaging (Fig. 1 – see Fig. S1 for BSE images of all MIs) and chemical characterisation of MIs and their host silicates in the studied Apollo samples were performed using the FEI Quanta 200 3D scanning electron microscope (SEM) and with the Cameca SX-100 electron microprobe (EPMA) at The Open University. Major-element mineral chemistry was measured using a 15 kV accelerating voltage and a 20nA current. The beam size was set to 1 μm for silicates and was defocused to 3 μm for MIs. The measured chemical compositions of MIs are presented in supplementary Table S2. The size of MIs ranges from 5 to 120 μm in diameter (cf. Table 1). In order to avoid potential migration of volatiles (Goldoff et al., 2012), EPMA analyses were performed after NanoSIMS analyses. However, because of the small sizes of most MIs, the cratered spots created during NanoSIMS analysis prevented or compromised EPMA data collection on most

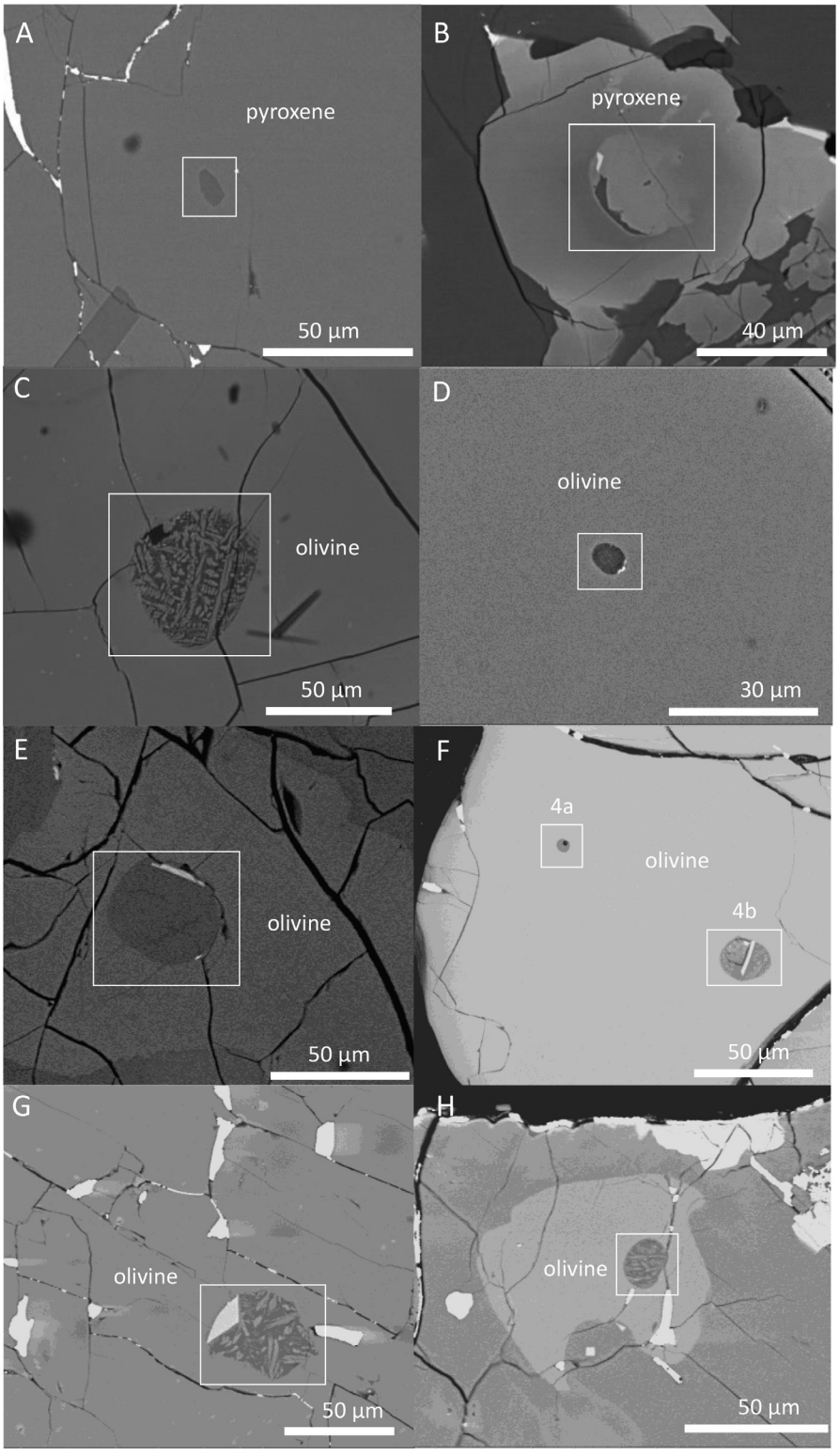


Fig. 1. A representative selection of BSE images for olivine-hosted and pyroxene-hosted MIs in the studied Apollo thin sections. (A) Pyroxene-hosted MI #5 in sample 10058; (B) Pyroxene-hosted MI #1 in sample 12002; (C) Olivine-hosted MI #27 in sample 12004; (D) Olivine-hosted MI #6B in sample 12008; (E) Olivine-hosted MI #10 in sample 12020; (F) Assemblage of two olivine-hosted MIs #4A and #4B in sample 12040. MI #4A shows a shrinkage bubble; (G) Olivine-hosted MI #15 in sample 14072; H) Olivine-hosted MI #23 in sample 15016.

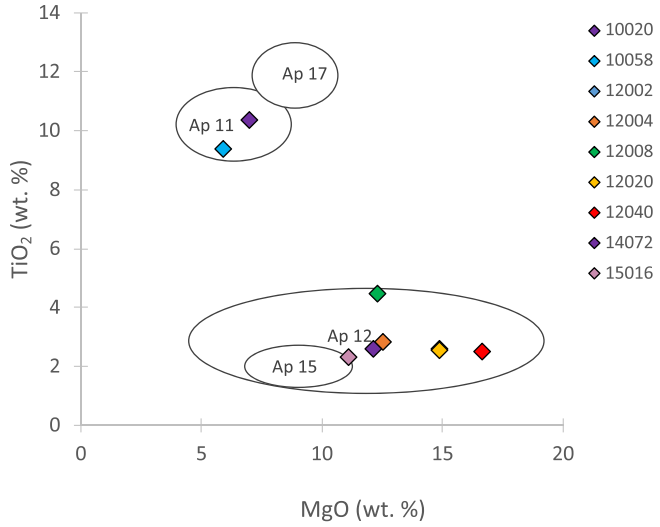


Fig. 2. Bulk-rock MgO vs $TiO_2$ composition of the studied Apollo samples. Bulk-rock compositions are from Rhodes and Blanchard (1980) for 10020 and 10058; Willis et al. (1971) for 12002; Maxwell and Wiik (1971) for 12004; Rhodes et al. (1977) for 12008; Kushiro and Haramura (1971) for 12020 and 12040; Taylor et al. (1972) for 14072; Rhodes and Hubbard (1973) for 15016. The full range of compositional variations recorded in basalts from Apollo collections studied here (Apollo 11, 12, 15 and 17) is highlighted using elliptical outlines.

MIs. Consequently, some EPMA analyses have low oxide totals (95 to 98%).

## 2.4. NanoSIMS

### 2.4.1. Melt inclusion measurements

Measurements of D/H and $H^-/^{18}O^-$ ratios (reported in terms of equivalent $H_2O$ concentrations) in the olivine- and pyroxene-hosted MIs were performed with the Cameca NanoSIMS 50L at The Open University in two sessions (10020, 12004, 12040, 14072 and 15016 during session 1; 10020, 10058, 12002, 12008, 12020 during session 2). The $H^-$, $D^-$, $^{13}C^-$ and $^{18}O^-$ secondary ions were measured using a $Cs^+$ primary beam of 550 pA. The ion $^{13}C^-$ was used to monitor any potential terrestrial contamination and any crack(s) in the analysis area. The primary beam was rastered over an 8 μm × 8 μm area. Each analysis surface area was divided into 64 × 64 pixels, with a counting time of 0.132 ms per pixel. Blanking was performed, and ion counts from only the 4 μm × 4 μm (25%) interior of the rastered areas were recorded, with each measurement consisting of 200 cycles. Prior to each analysis, the surface was pre-sputtered for ~2 min using the same primary beam current. Vacuum in the analytical chamber was maintained at or below $5 \times 10^{-10}$ Torr throughout both sessions. Samples were kept under high vacuum for at least 24 h prior to analysis. An electron gun was used for charge compensation and tuned to an electron current of ~1800nA. A $H^-/^{18}O^-$ vs. $H_2O$ calibration curve, based on analyses of DR5, DR15, and DR20 basaltic glasses, was used to determine $H_2O$ concentrations in MIs. Background for $H_2O$ concentrations was corrected using the average $H^-/^{18}O^-$ ratio of six analyses on San Carlos olivine, estimated to be 10 ± 2 μg/g and 13 ± 3 μg/g; for sessions 1 and 2, respectively. Errors estimated for $H_2O$ concentrations account for the errors from counting statistics, from the background estimation and from uncertainties on the calibration lines. Slopes of the calibration lines were calculated using the R programming language for statistical computing, which yielded 8.71 ± (0.63) × $10^{-5}$ (n = 17, ±2SD) and 1.18 (±0.11) × $10^{-5}$ (n = 12, ±2SD) for sessions 1 and 2, respectively (Fig. S2).

Most MIs in Apollo samples are partially crystallised. Hence, their measured volatile contents had to be corrected accordingly, using the established method of post-entrapment crystallisation (PEC) correction. We calculated the PEC percentage, i.e., the percentage of crystallised daughter minerals in the MI, in each case, using the Petrolog3 program, following the method described in Danyushevsky and Plechov (2011). The forsterite (Fo) contents (or Mg# of pyroxene) of host phenocrysts, coupled with their bulk-rock composition, were used to calculate the percentage of PEC in each case (c.f. Table S2). Using these PEC values, water abundances were corrected following equation (1):

$$H_2O_{corrected} = [(100\text{-}PEC\%)/100] \times H_2O_{measured} \quad (1)$$

The calculated PEC percentages alongside corrected water contents are given in Table 1, and the latter are used in the rest of the manuscript.

For hydrogen isotopic measurements, an IMF factor α of 1.10 ± 0.06 (session 1; n = 17, ±2SD) and 1.01 ± 0.05 (session 2; n = 12, ±2SD) was calculated based on repeated analyses of the MORB standards. The measured D/H ratios are expressed using the δD notation defined earlier. The raw measured D/H ratios were corrected for IMF, followed by corrections for the background and for the effects of spallation reactions, using a D production rate of 2.17 × $10^{-12}$ mol D/g/Ma (Füri et al., 2017). This production rate has been estimated based on $H_2O$-poor olivine and is appropriate for silicates and their MIs (see Füri et al., 2017). As such, all discussion on MIs in this manuscript

Table 1
Water content and hydrogen isotopic composition of lunar MIs in Apollo samples 10020, 10058, 12002, 12004, 12008, 12020, 12040, 14072, 15016. $H_2O$ measured and $H_2O$ corrected from PEC are included. $\delta D_{corrected}$ corresponds to δD corrected for IMF and background. $\delta D_{spallation}$ are corrected using the D production rate of Füri et al. (2017). PEC (%) correspond to the percentages of daughter minerals in the MIs and have been calculated using Petrolog3 (see text for details). Mg# of the host has been calculated as Mg# = Mg/(Mg + Fe). MI diameter has been measured taking the largest diameter of the MI.

| Sample/Host | MI # | $H_2O$ measured (μg/g) | $H_2O$ corrected (PEC) | 2σ | δD (‰) corrected | 2σ | δD (‰) spallation | 2σ | PEC (%) | Host Mg# | MI diameter (μm) |
|---|---|---|---|---|---|---|---|---|---|---|---|
| **10020,31** | | | | | | | | | | | |
| Olivine | MI 12 | 56 | 46 | 15 | 2236 | 610 | 1942 | 611 | 17 | 69.4 | 22 |
| Olivine | MI 13 | 50 | 32 | 13 | 1596 | 499 | 1265 | 501 | 36 | | 27 |
| Olivine | MI 22A | 29 | 14 | 8 | 2151 | 639 | 1585 | 643 | 52 | 70.9 | 53 |
| Pyroxene | MI 20A | 166 | 105 | 44 | −131 | 210 | −234 | 210 | 37 | 70.2 | 5 |
| Pyroxene | MI 20B | 230 | 145 | 60 | 70 | 229 | −4 | 229 | 37 | 70.2 | 5 |
| Olivine | MI 6A | 222 | 120 | 40 | 834 | 397 | 759 | 397 | 46 | 72.6 | |
| Olivine | MI 6B | 124 | 83 | 23 | 4 | 225 | −134 | 225 | 33 | 72.6 | |
| Olivine | MI 6C | 55 | 33 | 11 | −112 | 212 | −421 | 216 | 40 | 72.3 | |
| Olivine | MI 32 | 10 | 6 | 2 | 1057 | 531 | −646 | 578 | 45 | 71.7 | |
| Olivine | MI 10 | 366 | 161 | 65 | 579 | 338 | 533 | 338 | 56 | 72.5 | 26 |
| **10058,254** | | | | | | | | | | | |
| Pyroxene | MI3 | 115 | 66 | 16 | 22 | 271 | −58 | 271 | 42 | 72.6 | 27 |
| Pyroxene | MI5 | 252 | 212 | 27 | −133 | 222 | −169 | 222 | 16 | 74.5 | 12 |
| Pyroxene | MI7 | 6 | 6 | 1 | 764 | 500 | −912 | 553 | 39 | 75.9 | 23 |
| Pyroxene | MI6 | 130 | 95 | 32 | 64 | 281 | −7 | 281 | 27 | 35.3 | 15 |
| **12002,562** | | | | | | | | | | | |
| Olivine | MI 9A | 189 | 113 | 34 | 619 | 352 | 508 | 352 | 40 | 69.6 | |
| Olivine | MI 9B | 25 | 9 | 6 | 443 | 376 | −412 | 407 | 65 | 70.0 | |
| Olivine | MI 71 | 15 | 9 | 4 | 1356 | 665 | −55 | 717 | 43 | 71.6 | |
| Olivine | MI 73 | 63 | 25 | 13 | 354 | 321 | 18 | 328 | 60 | 60.2 | |
| Olivine | MI 82 | 46 | 12 | 10 | 715 | 416 | 260 | 425 | 73 | 70.7 | |
| Pyroxene | MI 34 | 16 | 9 | 4 | 2238 | 811 | 972 | 850 | 46 | 65.1 | |
| **12004,51** | | | | | | | | | | | |
| Olivine | MI 1 | 63 | 32 | 17 | 32 | 241 | −104 | 243 | 50 | 67.4 | 25 |
| Olivine | MI 13 | 39 | 15 | 10 | −275 | 212 | −496 | 219 | 63 | 69.6 | 75 |
| Olivine | MI 24A | 217 | 121 | 57 | 27 | 318 | −13 | 318 | 44 | 70.5 | 22 |
| Olivine | MI 24B | 38 | 14 | 10 | 64 | 285 | −164 | 290 | 62 | 73.0 | 19 |
| Olivine | MI 27 | 18 | 8 | 5 | 154 | 369 | −332 | 386 | 56 | 64.7 | 56 |
| Pyroxene | MI 16 | 63 | 36 | 17 | 209 | 340 | 73 | 342 | 43 | 66.3 | 20 |
| Pyroxene | MI 25 | 26 | 15 | 7 | 132 | 339 | −204 | 348 | 40 | 41.0 | 7 |
| **12008,18** | | | | | | | | | | | |
| Olivine | MI 2 | 15 | 8 | 4 | 265 | 342 | −185 | 362 | 47 | 68.9 | 10 |
| Olivine | MI 6 | 11 | 10 | 3 | 939 | 544 | 345 | 567 | 10 | 68.5 | 6 |
| Olivine | MI 8 | 141 | 90 | 26 | −118 | 196 | −165 | 196 | 36 | 67.0 | 34 |
| Olivine | MI 11-a | 38 | 28 | 8 | 315 | 320 | 142 | 323 | 27 | 68.4 | 32 |
| Olivine | MI 11-b | 119 | 87 | 23 | 142 | 259 | 87 | 260 | 27 | 68.4 | 32 |
| Olivine | MI 13 | 30 | 17 | 7 | 502 | 375 | 283 | 379 | 43 | 67.8 | 21 |
| Olivine | MI 14 | 132 | 121 | 24 | 96 | 242 | 46 | 243 | 8 | 68.9 | 16 |
| **12020,8** | | | | | | | | | | | |
| Olivine | MI 5A | 90 | 30 | 18 | 52 | 242 | −80 | 243 | 67 | 67.8 | 85 |
| Olivine | MI 5B | 54 | 18 | 11 | 277 | 295 | 57 | 299 | 67 | 67.8 | 85 |
| Olivine | MI 9 | 17 | 4 | 4 | 1531 | 636 | 834 | 657 | 74 | 74.4 | 34 |
| Olivine | MI 10 | 85 | 65 | 16 | 416 | 318 | 276 | 320 | 23 | 66.3 | 40 |
| Olivine | MI 11 | 29 | 16 | 6 | 546 | 372 | 134 | 384 | 46 | 69.1 | 20 |

(*continued on next page*)

Table 1 (*continued*)

| Sample/Host | MI # | $H_2O$ measured (μg/g) | $H_2O$ corrected (PEC) | 2σ | δD (‰) corrected | 2σ | δD (‰) spallation | 2σ | PEC (%) | Host Mg# | MI diameter (μm) |
|---|---|---|---|---|---|---|---|---|---|---|---|
| Olivine | MI 15 | 34 | 22 | 7 | 253 | 295 | −94 | 304 | 35 | 63.7 | 68 |
| Pyroxene | MI 2 | 38 | 20 | 8 | 342 | 313 | 32 | 321 | 49 | 66.2 | 22 |
| Pyroxene | MI 17 | 30 | 15 | 6 | 631 | 391 | 230 | 402 | 48 | 67.2 | 17 |
| **12040,44** | | | | | | | | | | | |
| Olivine | MI 2 | 117 | 77 | 31 | −72 | 185 | −393 | 200 | 34 | 52.3 | 23 |
| Olivine | MI 4A | 194 | 194 | 51 | −156 | 182 | −349 | 187 | 0 | 53.9 | 5 |
| Olivine | MI 4B | 50 | 33 | 13 | 234 | 334 | −520 | 376 | 34 | 53.9 | 19 |
| Olivine | MI 12 | 63 | 31 | 17 | 62 | 267 | −534 | 300 | 51 | 58.3 | 42 |
| Olivine | MI 16 | 30 | 15 | 8 | 656 | 493 | −597 | 570 | 49 | 58.2 | 36 |
| Olivine | MI 21A | 118 | 68 | 31 | −136 | 198 | −456 | 211 | 42 | 59.2 | 28 |
| Pyroxene | MI 24A | 22 | 12 | 6 | 171 | 362 | | *n.d.* | 46 | 73.3 | 17 |
| **14072,13** | | | | | | | | | | | |
| Olivine | MI 2A-a | 85 | 38 | 22 | −410 | 235 | −442 | 235 | 56 | 70.9 | 120 |
| Olivine | MI 2A-d | 125 | 55 | 33 | −244 | 225 | −266 | 225 | 56 | 70.9 | 120 |
| Olivine | MI 2B | 167 | 73 | 44 | −91 | 250 | −108 | 250 | 56 | 71.9 | 22 |
| Olivine | MI 15 | 47 | 14 | 12 | −308 | 277 | −368 | 278 | 70 | 76.3 | 42 |
| Olivine | MI 39 | 54 | 39 | 14 | −382 | 261 | −433 | 261 | 28 | 58.4 | 30 |
| **15016,14** | | | | | | | | | | | |
| Olivine | MI 23 | 14 | 8 | 4 | *1784* | *747* | *n.d.* | *n.d.* | 43 | 54.6 | 16 |
| Olivine | MI 35 | 3 | 2 | 1 | *8335* | *2662* | *n.d.* | *n.d.* | 25 | 43.8 | 21 |
| Pyroxene | MI 1 | 150 | 135 | 39 | 197 | 275 | −152 | 287 | 10 | 49.0 | 6 |
| Pyroxene | MI 9 | 112 | 84 | 29 | 145 | 232 | −325 | 257 | 25 | 52.6 | 6 |

uses spallation corrected δD values. Due to the low water contents measured in the studied MIs, the correction of δD values for spallation effects is significant for most samples, with the exception of 14072 which has a low CRE age of 21 Ma. Samples 12040 and 15016 have very long exposure ages at 285 ± 50 and 400 ± 73 Ma, respectively. As a result, the amount of D produced by spallation is significant, and therefore, MIs with $H_2O$ concentrations <25 μg/g have undetermined spallation-corrected hydrogen isotopic ratio. Uncertainties associated with δD values include uncertainties in counting statistics as well as in IMF estimation, in background δD values, and in spallation corrections. All NanoSIMS spots were checked after analysis using SEM imaging to confirm that analyses targeted the MI and not the surrounding host minerals. The full MI dataset is presented in Table 1.

### 2.4.2. Apatite measurements

The $H^-/^{18}O^-$ ratio and H isotope composition of a number of apatite grains in samples 10020, 12002, 12004, 12040 and 14072 were measured, in two different sessions, using a Cameca NanoSIMS 50L at The Open University, following the protocol detailed in Barnes et al. (2013) and Tartèse et al. (2013). In brief, a large $Cs^+$ primary beam of *ca*. 250 pA current with an accelerating voltage of 16 kV was rastered on the sample surface over 12 μm × 12 μm area during a 3 min pre-sputter to eliminate any surface contamination. For analysis, secondary ions of $^1H^-$, $^2H^-$, $^{12}C^-$ and $^{18}O^-$ were collected simultaneously from the central areas of 6 μm × 6 μm to 10 μm × 10 μm rasters, with a 25% blanking on electron multipliers, for ~10 min. An electron gun was used for charge compensation and tuned to minimise its contribution to the background H. The ion $^{12}C^-$ was used to monitor any potential terrestrial contamination and cracks during analyses. The mass resolving power was set to ~4000, sufficient to readily resolve $^2H^-$ from molecular $H_2^-$. Vacuum in the analytical chamber was maintained at or below $5 \times 10^{-10}$ Torr during both sessions. Samples were kept under high-vacuum for at least 24 h prior to analysis.

Apatite $H_2O$ contents were calibrated using the measured $^1H$-/$^{18}O$- ratio and the calibrations derived using reference apatite samples with known $H_2O$ contents, comprising Ap003 (600 ± 400 μg/g $H_2O$), Ap004 (5500 ± 500 μg/g $H_2O$), and Ap018 (2000 ± 400 μg/g $H_2O$) (McCubbin et al., 2012). Two distinct sessions were necessary to perform apatite measurements. Samples 12040 and 14072 were analysed during session 1 and samples 10020, 12002, and 12004 were analysed during session 2. The uncertainties on the slopes of the calibration lines used to calculate apatite $H_2O$ contents were ±5.8% and ±5.0% (95% confidence interval) for the first and second session, respectively (Fig. S3). During the first session, background $H_2O$ of 14 ± 8 μg/g (2σ) was estimated based on repeat analysis of San Carlos olivine (n = 8) and was subtracted from the measured $H_2O$ in Apollo samples. Measured D/H ratios were corrected for IMF using repeat analysis of Ap004 (δD = −45 ± 5‰, McCubbin et al., 2012), which

Table 2
Water content and hydrogen isotopic composition of lunar apatite in Apollo samples 10020, 10058, 12002, 12004, 12040, 14072. δD values are IMF and background corrected. δD values are reported after spallation correction using the D production rate of Merlivat et al. (1976). Throughout this paper, all δD values reported from this work are corrected for spallation.

| Sample | Apatite # | $H_2O$(μg/g) | 2σ | δD (‰) corrected | 2σ | δD (‰) spallation | 2σ |
|---|---|---|---|---|---|---|---|
| **14072,13** | | | | | | | |
| | Ap1 | 323 | 19 | 116 | 230 | 112 | 230 |
| | Ap2#1 | 68 | 4 | 325 | 341 | 306 | 341 |
| | Ap2#2 | 93 | 5 | 151 | 323 | 137 | 323 |
| | Ap3 | 81 | 5 | 27 | 410 | 10 | 410 |
| | Ap4 | 265 | 15 | 147 | 345 | 142 | 345 |
| | Ap5 | 74 | 4 | 452 | 308 | 434 | 308 |
| **12040,44** | | | | | | | |
| | Ap1#1 | 38 | 4 | 633 | 349 | 437 | 377 |
| | Ap1#2 | 51 | 5 | 132 | 355 | −17 | 369 |
| | Ap3#1 | 25 | 2 | 603 | 366 | 298 | 426 |
| | Ap3#2 | 61 | 6 | 172 | 393 | 47 | 403 |
| | Ap3#3 | 63 | 6 | 324 | 306 | 204 | 317 |
| | Ap4#1 | 40 | 4 | 195 | 330 | 5 | 355 |
| | Ap4#2 | 44 | 4 | 189 | 372 | 16 | 391 |
| | Ap6#1 | 75 | 7 | 304 | 246 | 203 | 256 |
| | Ap6#2 | 91 | 9 | 206 | 555 | 122 | 558 |
| **10020,31** | | | | | | | |
| | Ap1 | 1440 | 251 | 599 | 339 | 595 | 339 |
| **12002,562** | | | | | | | |
| | Ap 1 | 794 | 59 | 579 | 235 | 568 | 235 |
| | Ap 2 | 1286 | 91 | 1108 | 306 | 1102 | 306 |
| **12004,51** | | | | | | | |
| | Ap 1 | 746 | 56 | 965 | 291 | 961 | 291 |

yielded an IMF of 251 ± 50‰ (2σ, n = 8). For the second session, the background estimated from San Carlos olivine analyses was 44 ± 6 μg/g $H_2O$ (2σ, n = 4) whereas the IMF was 100 ± 42‰ (2σ, n = 4).

The IMF- and background-corrected δD values were corrected for the effects of spallation reactions, using a D production rate of $9.20 \times 10^{-13}$ mol D/g/Ma (Merlivat et al., 1976). As apatite in samples 10020, 12004 and 12020 have relatively higher water contents (>700 μg/g $H_2O$), the spallation correction is negligible (maximum shift in δD values by 11‰, which is within the overall measurement uncertainty of δD values). Apatite in 14072 and 12040 have much lower water contents. However, 14072 has a CRE age of 21 Ma. Therefore, the spallation correction for 14072 apatite is also negligible (shift in δD values by < 20‰). Because 12040 has an extremely old CRE age (285 ± 50 Ma), the associated spallation corrections result in significant changes in δD values. Thus, we caution against overinterpreting the data for 12040, especially keeping in mind that spallogenic D production rates for apatite have not yet been determined. All discussion on apatite δD in this work from here on refers to spallation corrected δD values.

The apatite $H_2O$ contents and δD values are reported with their 2 σ uncertainties in Table 2, which include the reproducibility obtained on repeated analysis of Ap004, the internal precision of each analysis, and the uncertainties associated with cosmic-ray spallation correction.

## 3. RESULTS

### 3.1. Chemistry of melt inclusions

The major-element composition of MIs (uncorrected for PEC) are displayed in Fig. 3 (Fig. S4). These plots illustrate the compositional evolution of the parental melts in each case. Data for homogenised MIs (from Chen et al., 2015) are plotted along with our data for crystallised MIs. Homogenised MIs plot within the range defined by bulk-rock composition, while crystallised MIs display a large range in composition, revealing the evolution of the parent melt at their time of trapping. Major-element compositions suggest that the studied MIs could have potentially recorded a larger span of melt crystallisation, and thus represent a snapshot of melt composition at the time of their trapping. Indeed, the original composition of MIs were also affected by PEC. It is interesting to note that MI 6 hosted in pyroxene in sample 10058 has a very high $SiO_2$ content of 90 wt. %. This is most probably an evidence of silicate liquid immiscibility as this glass inclusion is near a plagioclase, which have been observed previously in Apollo 11 rocks (Roedder and Weiblen, 1970).

A major concern regarding MIs is the possibility that they have re-equilibrated with their host during natural cooling. This re-equilibration manifests itself as Fe-loss from the MIs (Danyushevsky et al., 2002; Kent 2008 and refs therein). If the MIs in Apollo basalts had undergone

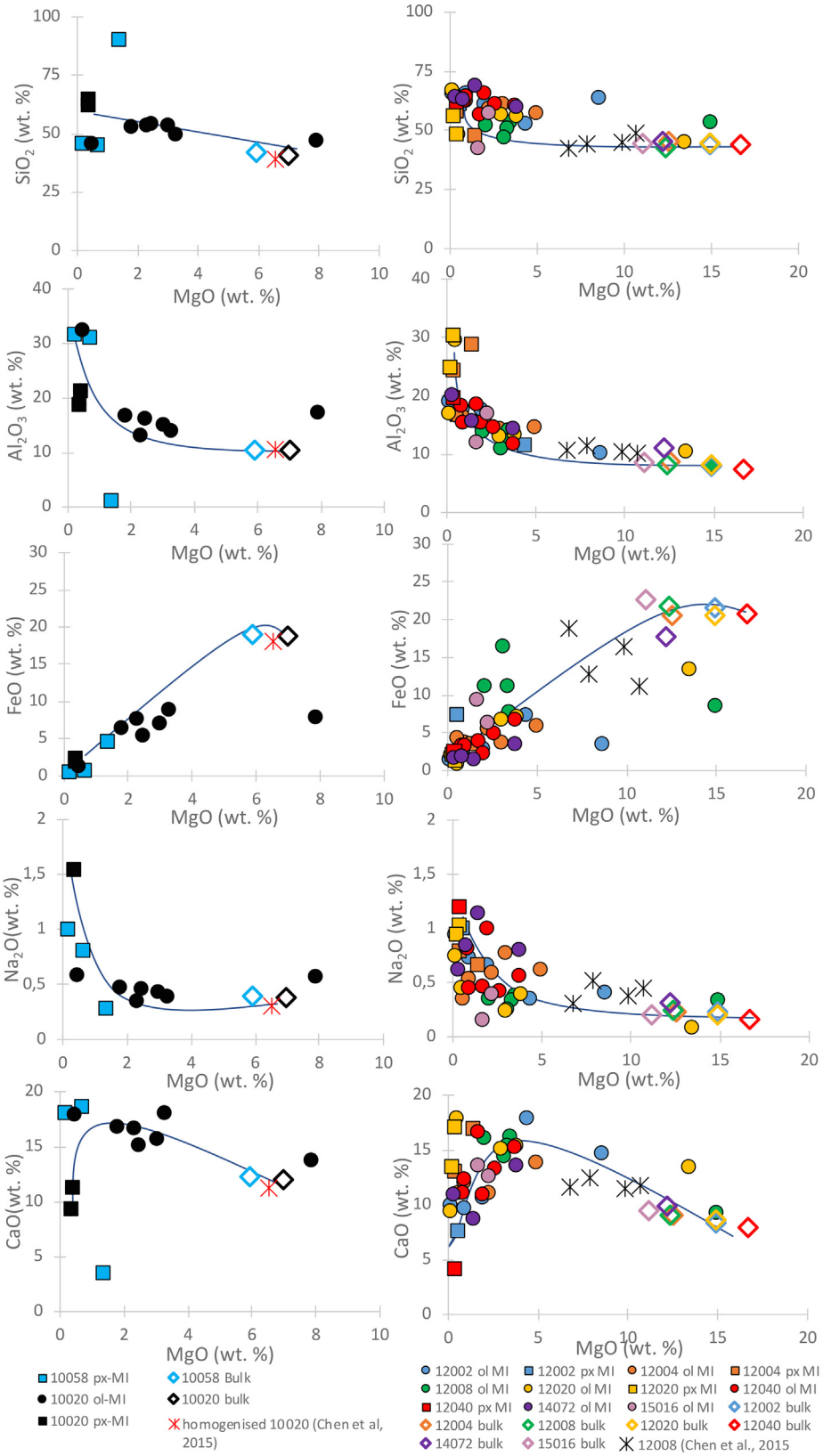


Fig. 3. Major-element composition of MIs (uncorrected for PEC) and bulk-rock samples, expressed in terms of oxide weight% (wt%). The high-Ti basalts (10020 and 10058) are plotted in the left column whereas the low-Ti basalts (Apollo 12002, 12004, 12008, 12020, 12040, 14072 and 15016) are plotted in the right column. Data from Chen et al. (2015) on homogenised MIs from 10020 and 12008 are also plotted for comparison purposes. Blue lines represent predicted liquid lines of descent.

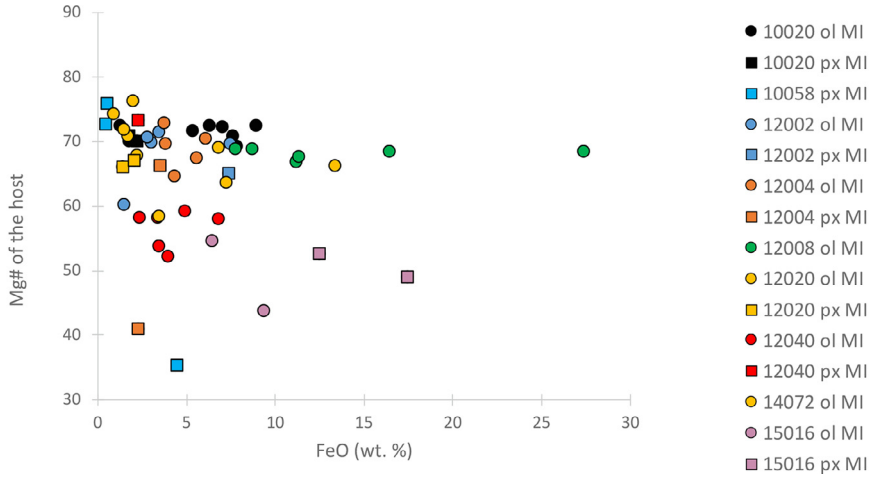


Fig. 4. Melt-inclusion host phenocryst Mg# vs. MI FeO abundance (uncorrected for PEC). Mg# is defined as the mole fraction Mg/(Fe + Mg).

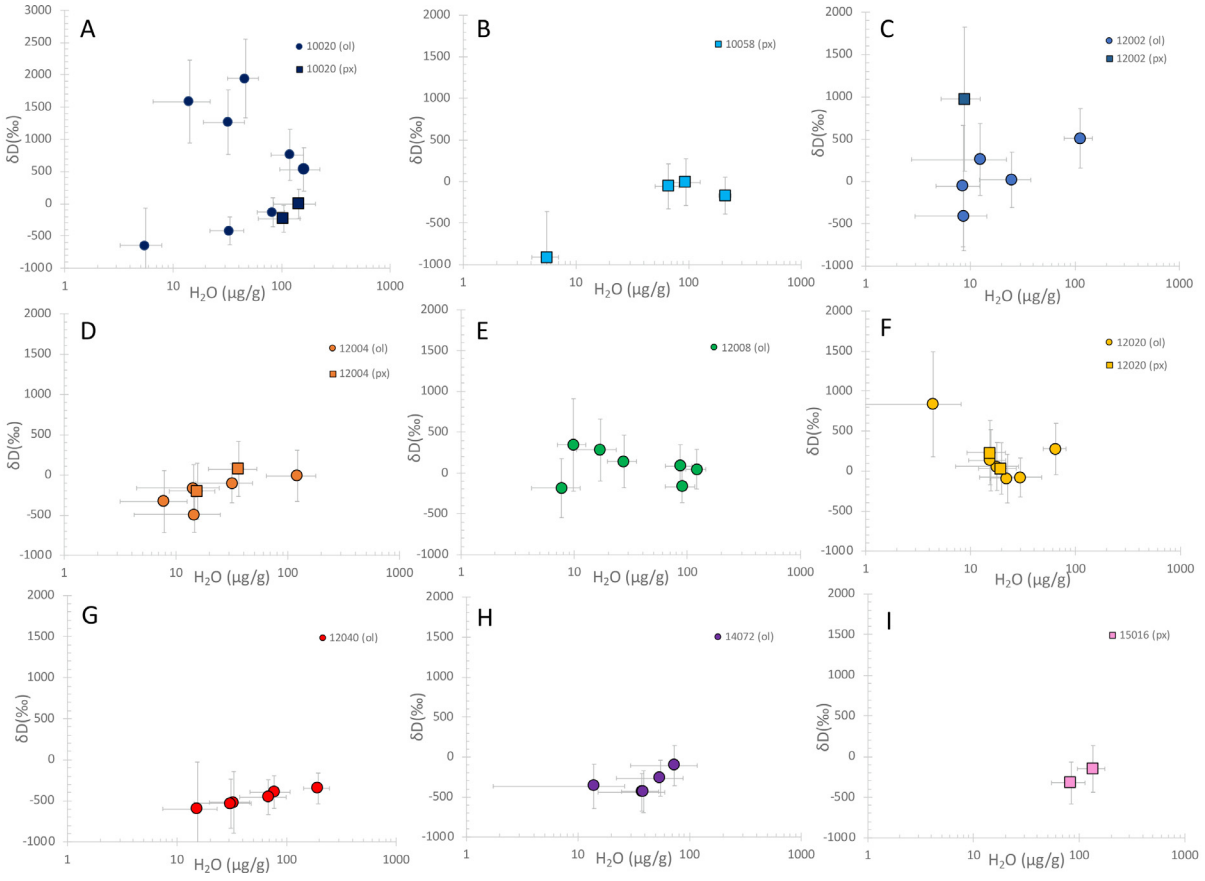


Fig. 5. δD (‰) vs. $H_2O$ (µg/g) in silicate melt inclusions for each Apollo sample studied here: (A) 10020, (B) 10058, (C) 12002, (D) 12004, (E) 12008, (F) 12020, (G) 12040, (H) 14072, (I) 15016. Data points represented by a circle or a square represent either an olivine-hosted or pyroxene-hosted MI, respectively. $H_2O$ contents represented here are corrected for PEC; δD values are corrected for spallation using the production rate of Füri et al. (2017). Please note that y-axis for 10020 (graph A) is different than the other graphs.

such Fe loss, their composition would plot below the liquid line of descent predicted from bulk-rock FeO vs. MgO (c.f. Fig. 3). Similarly, a negative correlation between the Mg# of the host and FeO content of an inclusion should be seen as a result of Fe-loss during re-equilibration between olivine and melt (Yaxley et al., 2004; Kent et al., 2008) (c.f. Fig. 4).

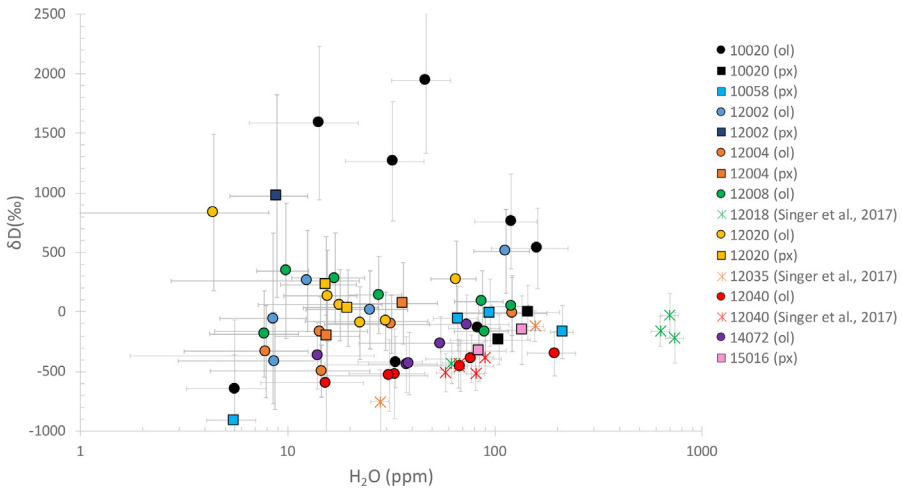


Fig. 6. δD (‰) vs $H_2O$ (μg/g) in silicate melt inclusions for all samples in this study plotted together with the literature data from Singer et al. (2017). For MIs analysed in this study, $H_2O$ contents are corrected for PEC and δD values are corrected for spallation using the production rate of Füri et al. (2017). Round and square symbols are for olivine-hosted MI and pyroxene-hosted MI, respectively. Star symbols refer to Singer et al. (2017) MI data on samples 12018, 12035 and 12040, corrected for spallation using the production rate of Füri et al. (2017).

Neither of these two characteristics apply for the large majority of the MIs in the studied Apollo basalts, arguing against a re-equilibration of the MIs with their host crystals.

### 3.2. Water content and hydrogen isotopic ratios

#### *3.2.1. 10020*

Eight olivine-hosted MIs and two pyroxene-hosted MIs were analysed in sample 10020. These inclusions have a PEC values between 17 and 56%. After PEC correction, $H_2O$ contents range from $6 \pm 2$ to $161 \pm 65$ μg/g. Hydrogen isotopic composition of olivine-hosted MIs show a very large range of δD values from $-646 \pm 578$ to $+1942 \pm 611$‰. In contract, the pyroxene-hosted MIs have more restricted δD values of $-234 \pm 210$ and $-4 \pm 229$‰. Interestingly, $H_2O$-δD systematics in 10020 MIs seem to follow two opposite trends (Fig. 5A and Fig. 6). The $R^2$ values are 0.74 and 0.90, for the negative and the positive trends, respectively. The MI with the highest $H_2O$ content (i.e., 161 μg/g) is associated with a δD value of $+533 \pm 338$‰.

A single analysis in apatite yielded a water concentration of $1440 \pm 251$ ppm and an associated δD value of $+595 \pm 339$‰ (Fig. 7).

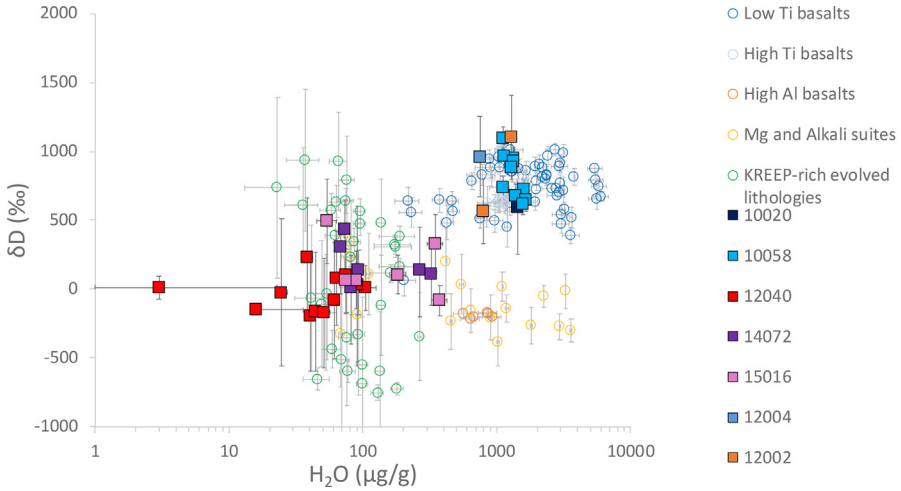


Fig. 7. Apatites $H_2O$-δD systematics, in μg/g and permil, respectively. The data plotted for samples 10020, 12002, 12004, 12040 and 14072 are from this study. Data for 10058 and 15016 are from Tartèse et al. (2013) and Barnes et al. (2019), respectively. Samples 10020 and 10058 are high-Ti basalts while the others are low-Ti basalts. Literature data for apatite from low-Ti and high-Ti basalt are from Greenwood et al. (2011), Barnes et al. (2013), Tartèse et al. (2013), Boyce et al. (2015); high-Al basalt apatite are from Greenwood et al. (2011); for Mg- and Alkali-suite apatite are from Greenwood et al. (2011) and Barnes et al. (2014); QMD evolved lithologies apatite are from Robinson et al. (2016). δD values of 10058, 12002, 12004, 12040, 14072 and 15016 are corrected for spallation using the production rate of Merlivat et al. (1976), in order to compare our data with the literature data on lunar apatite.

*3.2.2. 10058*

Sample 10058 is devoid of olivine phenocrysts. As such, only seven pyroxene-hosted MIs were identified in the 10058 thin section, four of which were analysed. The measured $H_2O$ concentration ranges from $6 \pm 1$ to $212 \pm 27$ μg/g, after PEC correction (16 to 42 % PEC). δD values in these MIs range from $-912 \pm 553$ to $-7 \pm 281$‰. The MI with the highest $H_2O$ content (i.e., 212 μg/g) is associated with a δD value of $-169 \pm 222$‰ (Fig. 5B).

Tartèse et al. (2013) analysed apatite grains in sample 10058 and reported water concentration of ~ 1350 ± 400 μg/g (2sd) with associated δD values ranging between 600 and 1100‰ (Fig. 7).

*3.2.3. 12002*

In sample 12002, MIs yielded a slightly more restricted range of water contents from $9 \pm 4$ to $113 \pm 34$ μg/g $H_2O$ (40 to 73 % PEC). The five olivine-hosted MIs and the one pyroxene-hosted MI have δD values covering a range from $-412 \pm 407$ to $+972 \pm 850$‰. The δD value of $+508 \pm 352$‰ of the MI with the highest $H_2O$ content (113 μg/g) is similar to that in 10020 (Fig. 5C).

Two apatite grains were analysed and yielded water concentrations of $794 \pm 59$ μg/g and $1286 \pm 91$ μg/g, with δD values of $568 \pm 235$‰ and $1102 \pm 306$‰ (Fig. 7).

*3.2.4. 12004*

Seven MIs were measured in 12004, among which five were in olivine and two in pyroxene. These MIs yielded a water content from $8 \pm 5$ μg/g to $121 \pm 57$ μg/g (40 to 63% PEC) (Fig. 5D). The δD values range from −496 ± 219‰ to + 73 ± 342‰. In this case also, the highest δD value was measured in a pyroxene-hosted MI. The highest water content of 121 μg/g is also similar to that measured in MI in 12002 and is associated with a δD value of −13 ± 318‰.

A single apatite analysis yielded a $H_2O$ abundance of $746 \pm 56$ μg/g and a δD value of $961 \pm 291$‰ (Fig. 7).

*3.2.5. 12008*

Six olivine-hosted MIs were analysed in 12008, with MI #11 being analysed twice (11a and 11b) in order to test any heterogeneity in δD and $H_2O$ in a crystallised MI. MIs in 12008 have relatively lower percentages of PEC between 8 and 47%. The $H_2O$ contents range from $8 \pm 4$ μg/g to $121 \pm 24$ μg/g and δD values from $-185 \pm 362$‰ to 345 ± 567‰ (Fig. 5E). The two analyses in MI #11 yielded $H_2O$ abundances of 28 and 87 μg/g, which can be explained by a different proportion of crystals and melt in the area analysed. However, the δD values of the two analyses are similar within errors, i.e., $87 \pm 260$ and $142 \pm 323$‰, which gives confidence in the broad reproducibility of δD measurements in partially crystallised MIs. The olivine-hosted MI with the highest water content (121 μg/g) has a δD value of $+46 \pm 243$‰.

*3.2.6. 12020*

Six olivine-hosted MIs and two pyroxene-hosted MIs yielded water contents from $4 \pm 4$ μg/g to $65 \pm 16$ μg/g, with percentage of PEC varying between 23 and 74%. The δD values range from $-94 \pm 304$‰ to $+834 \pm 657$‰. The olivine-hosted MI #10, which yielded 65 μg/g $H_2O$, has the lowest percentage of PEC (23%) and as an appearance of an almost glassy MI (Fig. 5F). It is associated with a δD value of $+276 \pm 320$‰.

*3.2.7. 12040*

In 12040, one pyroxene-hosted MI and six olivine-hosted MIs were analysed, among which one is glassy (although with a shrinkage bubble – Fig. 1). The $H_2O$ contents in olivine-hosted MIs range between $15 \pm 6$ μg/g and $194 \pm 51$ μg/g, while the pyroxene-hosted MI yielded 12 μg/g $H_2O$. The δD values range from $-597 \pm 570$‰ to −349 ± 187‰ (Fig. 5G). The low $H_2O$ content measured in the pyroxene-hosted MI in 12040 precluded calculation of a reliable δD value because of the sample's long CRE age of $285 \pm 50$ Ma. The glassy MI #4A contains the highest water concentration and is associated with a δD of −349 ± 187‰.

Nine measurements were performed on four apatite grains. Their water abundances range from $25 \pm 2$ to 91 ± 9 μg/g while the associated δD values range from −191 ± 404‰ to + 232 ± 429‰ (Fig. 7), which is consistent with previously reported D/H measurements in apatite in 12040 that range from $-150 \pm 26$‰ to $+27 \pm 91$‰ (Greenwood et al., 2011; Boyce et al., 2015), although these literature values are uncorrected from spallation correction.

*3.2.8. 14072*

Five analyses were performed in four olivine-hosted MIs in sample 14072. The measured water concentrations range from $14 \pm 12$ μg/g to $73 \pm 44$ μg/g (28 to 70% PEC) while the associated δD values range from $-442 \pm 235$‰ to $-108 \pm 250$‰ (Fig. 5H). Sample 14072 has a very short CRE age of ~ 21 Ma. The correction from D- produced by spallation is thus limited to a maximum of ca. 50‰. The MI with the highest water content records the highest δD value (i.e., $-108 \pm 250$‰).

Five apatite grains have also been analysed (Table 2) and yielded a range of $H_2O$ contents from $68 \pm 4$ μg/g to $323 \pm 19$ μg/g, with δD values ranging from $+13 \pm 410$‰ to $+437 \pm 308$‰ (Fig. 7).

*3.2.9. 15016*

In 15016, two olivine-hosted MIs and two pyroxene-hosted MIs were analysed. Water abundances measured in the olivine-hosted MIs are very low, between $2 \pm 1$ μg/g and $8 \pm 4$ μg/g $H_2O$ (10 to 43% PEC). Because sample 15016 has a very long CRE age of ~ 400 ± 73 Ma (Füri et al., 2017), no reliable spallation corrected δD values could be calculated. Pyroxene-hosted MIs contain between $84 \pm 29$ μg/g and $135 \pm 39$ μg/g $H_2O$, with associated δD values of $-325 \pm 257$‰ and $-152 \pm 287$‰, respectively (Fig. 5I).

Barnes et al. (in press) analysed apatite in samples 15016 and reported water concentrations ranging from 55 to 379 μg/g with associated δD values ranging between $-83 \pm 107$‰ and $+494 \pm 306$‰ (Fig. 7).

### 3.3. Link between the volatile composition of MI and their petrography and chemistry

The estimated water contents in MIs are plotted against the Mg# of their host and against the MI diameter (Fig. 8). A negative correlation between the MI water content and the Mg# of its host should indicate the relative time of entrapment of the MIs, since Mg# of olivine and pyroxene would decrease with progressive melt crystallisation while H should increase as it is incompatible in all major rock-forming silicate (e.g., olivine, pyroxene, plagioclase). It is important to note that this is true only if no other magmatic or secondary processes have altered the water content of MIs, post entrapment. Among all the MIs analysed in this study, the water contents in some of the Apollo 12 MIs show this expected correlation with their hosts' Mg# (Fig. 8A). The most notable trend is seen for ol-hosted MIs in 12040 (Fig. 8A) where the highest water content was measured in a MI trapped in olivine with the lowest Mg#. This may imply that, overall, MIs in 12040 formed from a more evolved parental melt compared to parental melts for other Apollo 12 samples. In contrast, the estimated water content in MIs from samples 10020 and 10058, as well as 14072 and 15016 do not show any such correlation with their host Mg#. Although a heterogeneity in melt composition cannot be ruled out, it is also possible that some other process may have erased the effect of crystallisation on MI water content in these cases. Regardless of either possibilities, it is interesting to note that at comparable host Mg#, the MIs are more water-rich in Apollo 11 samples compared to those in Apollo 12 samples (Table 1Fig. 8). However, no correlation is obvious between the host Mg# and the δD measured in MIs (Fig. 8D), which is consistent with the fact that no significant isotopic fractionation is expected during basaltic melt crystallisation (Kyser and O'Neil, 1984; Bindeman et al., 2012).

Previous studies have demonstrated a dependence of the water content in MI with the MI radius as a result of a more rapid re-equilibration among small MIs (<25 μm) compared to larger ones (Chen et al., 2013; Ni et al., 2017). This trend is not observed among the MIs studied here (Fig. 8C and D). However, Chen et al. (2013) and Ni et al. (2017) predominantly observed this correlation in the case of homogenized MI in which H diffusion was most likely enhanced during homogenisation experiments.

## 4. DISCUSSION

### 4.1. Reliability of $H_2O$-δD systematics in lunar MIs

Because MIs are the best available tool for assessing volatiles signatures of the primary basaltic magmas, numerous studies have examined various processes that can influence their original signatures subsequent to entrapment in a silicate-host. The modification of the original volatile inventory of MIs is principally caused by re-equilibration between the MI and an external melt, the composition and oxidation state of which changes during ascent and eruption (Mackwell and Kohlstedt, 1990; Kohlstedt and Mackwell, 1998; Hauri, 2002; Demouchy and Mackwell, 2006; Gaetani et al., 2012; Bucholz and Gaetani, 2013; Le Voyer et al., 2014). Small MIs are more susceptible to mod-

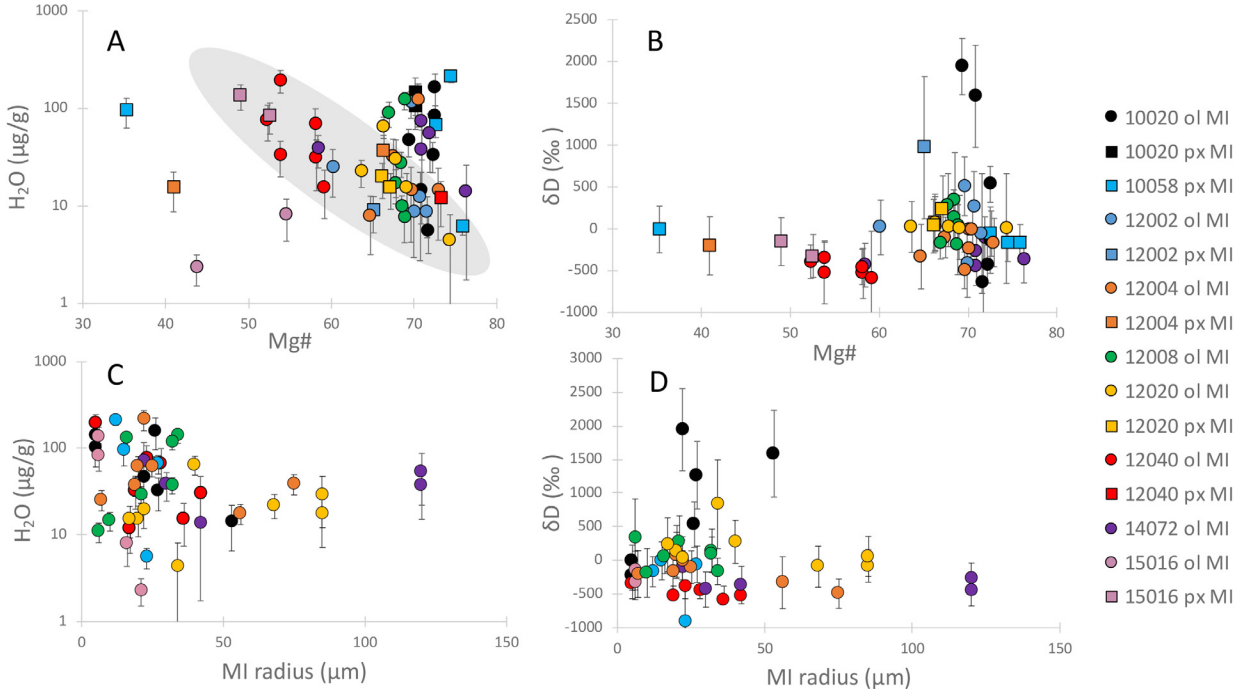


Fig. 8. $H_2O$ content (μg/g) and δD values (‰) of MIs in Apollo samples compared to Mg# of their host (Mg# is defined as the mole fraction Mg/(Fe + Mg)) and the diameter of the MI (μm). The grey shading emphasises the correlation between $H_2O$ content in MIs and their host #Mg for Apollo 12 basalts.

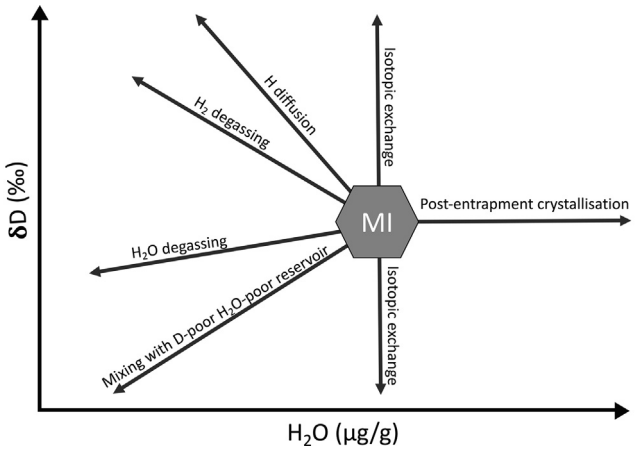


Fig. 9. A pictorial representation of the various processes that can alter the δD-$H_2O$ systematics of a lunar melt inclusion, post entrapment. See text for further discussion.

ification (Bucholz and Gaetani, 2013; Chen et al., 2013; Ni et al., 2017), which is the case for lunar MIs. Moreover, the large variations documented for both δD values and $H_2O$ abundances among the lunar MIs, as well as some trends observed in $H_2O$-δD systematics (Fig. 5), suggest that some processes have altered the primordial H inventory and isotope signature of these MIs. Hauri (2002) compiled an exhaustive list of such typical processes for terrestrial MIs, and here we will evaluate our measurements in light of some of these processes to assess whether lunar MIs are faithful recorders of lunar $H_2O$-δD systematics. These processes include post-entrapment growth of daughter crystals, (e.g., Danyushevsky et al., 2002; Steele-MacInnis et al., 2011), formation of vapour bubbles within inclusions (Moore et al., 2015), diffusive loss of H through the host (Gaetani et al, 2012; Bucholz and Gaetani, 2013), isotopic exchange with another H reservoir (Shaw et al., 2008), and shallow level degassing of melt prior to entrapment (Hauri, 2002). Most of these processes, which occur during ascent and eruption of basaltic magma, result in positive and negative trends between $H_2O$ abundances and δD values. These trends are pictorially represented in Fig. 9. Some of these processes require different speciation of H that can be found in lunar melt (Elkins-Tanton and Grove, 2011; Renggli et al., 2017; Dalou et al., 2019). Another important factor to take into consideration is an exogenous process that can also alter the primordial δD-$H_2O$ systematics of lunar material, namely solar wind implantation (Keller and McKay, 1997; McCord et al., 2011). Therefore, recognising such negative and positive trends in MI $H_2O$-δD dataset, and comparing them against various modelled curves, should allow estimation of the initial $H_2O$-δD systematics of the parental melts of the studied samples.

### 4.2. Basalt crystallisation

Before looking at magmatic and secondary processes that could induce hydrogen isotopic fractionation, the effect of melt crystallisation needs addressing, as it is often involved in giving rise to a range in $H_2O$ contents among MIs, from a single sample, if they are trapped at different stages of magma evolution. Indeed, the incompatibility of hydrogen in nominally anhydrous mineral increases the water content in the remaining melt. MIs trapped later in the crystallisation sequence are thus expected to be more water-rich than earlier-trapped MIs. A negative correlation between $H_2O$ content of MIs and their host Mg# is observed among some Apollo 12 basalt samples (cf. Fig. 8A). This correlation suggests that $H_2O$ contents in MIs from Apollo 12 basalts were mostly governed by the fractional crystallisation of their parental melts (see Fig. 10B). As such, the δD-$H_2O$ systematics of MI trapped in a host with the highest Mg# in Apollo 12 samples would therefore be closest to their initial parental melt volatile signature. For other samples (10020, 10058, 14072, 15016) which do not show such a correlation, other additional processes might have been involved. In these cases, the volatile-richer MI would be chosen as reflecting the initial melt, which for Apollo 11 samples match with high Mg# of silicate hosts.

### 4.3. Post-entrapment crystallisation (PEC)

Due to the relatively slow cooling rates of lunar melts (Holness et al., 2012; Walker et al., 1976; Tikoo et al., 2012), most of the MIs found in mare basalts are partially crystallised (Roedder, 1984). The formation of daughter minerals in MIs is characterised by some compositional changes causing Fe-loss: olivine crystallises on the inclusion wall and re-equilibrates with the host, typically resulting in a net Fe-loss in the trapped melt and an enrichment in the host (Danyushevsky et al., 2002; see EPMA data in supplementary Table S2). However, the elemental composition of the studied MIs and their hosts do not suggest that extensive Fe-loss from the trapped melt occurred (Yaxley et al., 2004; Kent et al., 2008) (Fig. 4).

The $H_2O$ contents measured in partially crystallised MIs have been corrected for their PEC percentages, as the crystallisation of anhydrous daughter minerals would have resulted in an increase in the water concentration of the remaining melt (Hauri, 2002) (see methods; Table 1). In term of δD measurements, Riciputi and Greenwood

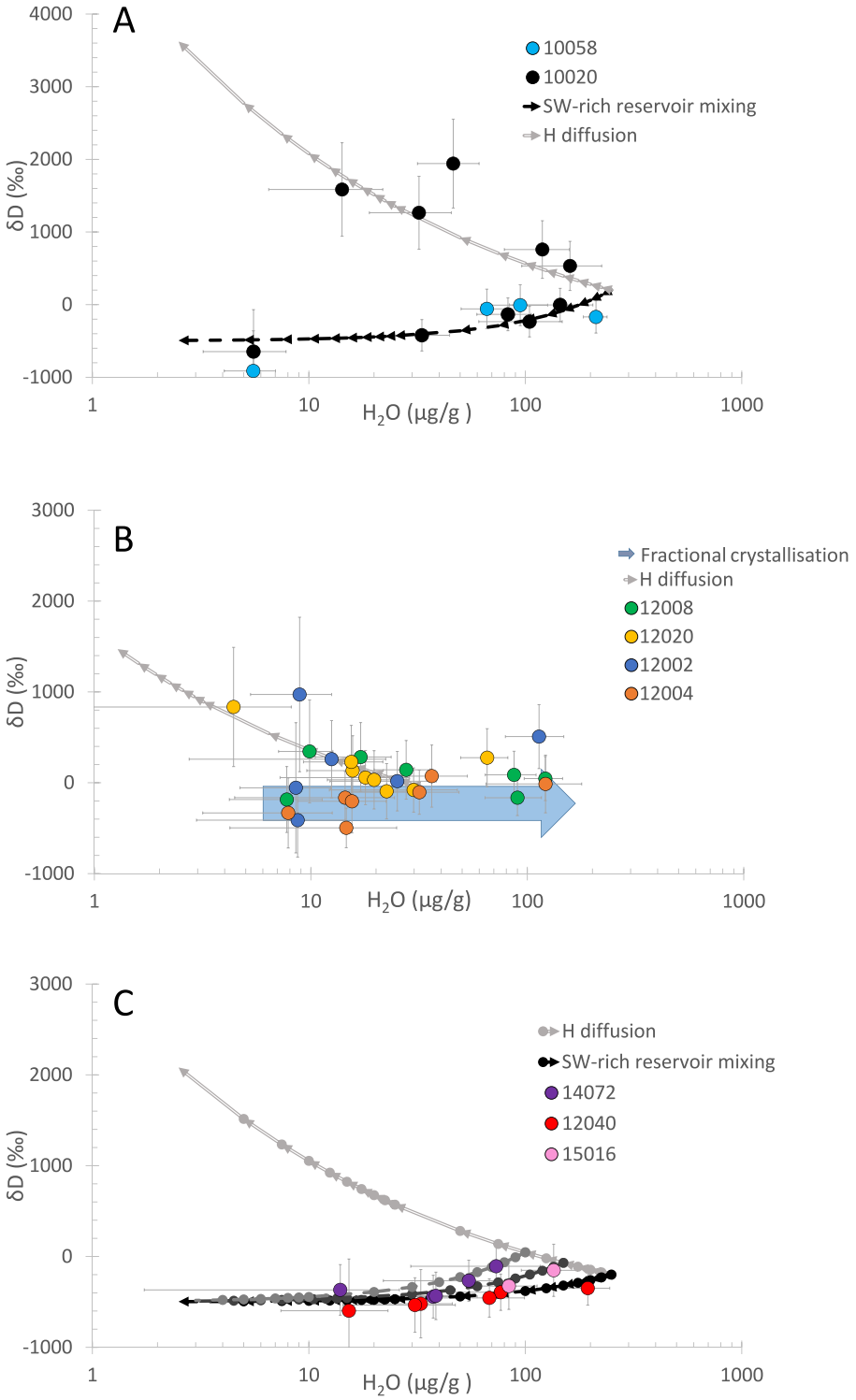


Fig. 10. Processes modifying the $H_2O$-δD systematics of lunar MIs. Also see Fig. 9 for a schematic of all possible processes and their trends. $H_2O$ contents represented here are corrected for PEC; δD values are corrected for spallation using the production rate of Füri et al. (2017). (A) Apollo 11 basaltic samples 10020 and 10058. Apollo 10020 MIs plot along two trends, $H^+$ diffusion through the host (light grey curves) and mixing with a D-poor reservoir (δD = −500‰) (black dashed curves). (B) Apollo 12 basaltic suite (samples 12002, 12004, 12008, 12020). MIs follow a trend defined by fractional crystallisation (blue arrow). Few MIs are also affected by $H^+$ diffusion (light grey curves). (C) Apollo low-Ti samples 12040, 14072 and 15016. All these samples fall on a mixing trend with a solar wind rich reservoir (δD = −500‰) (black dashed curves). See text for details. (For interpretation of the references to colour in this figure legend, the reader is referred to the web version of this article.)

Table 3
Comparison between water contents, estimated using crystallised and homogenised MIs from Apollo samples 10020, 12008, 12040 and 15016 in different studies. Our data for $H_2O$ content are PEC corrected.

| Sample | MI analysed | $H_2O$(μg/g) | References |
|---|---|---|---|
| **10020** | | | |
| | Homogenised MI | 131 ± 7 | Chen et al. (2015) |
| | Crystallised MI | 2.4 ± 0.1 to 346 ± 17 | Chen et al. (2015) |
| | Crystallised MI | 6 ± 2 to 161 ± 65 | *This study* |
| **12008** | | | |
| | Homogenised MI | 2.9 ± 0.1 to 77 ± 4 | Chen et al. (2015) |
| | Crystallised MI | 5.3 ± 0.3 to 40 ± 2 | Chen et al. (2015) |
| | Crystallised MI | 8 ± 4 to 121 ± 24 | *This study* |
| **12040** | | | |
| | Homogenised MI | 7.1 ± 1 to 14.2 ± 3 | Ni et al. (2019) |
| | Crystallised MI | 7.4 ± 1 to 33 ± 7 | Ni et al. (2019) |
| | Crystallised MI | 27 ± 3 to 90 ± 9 | Singer et al. (2017) |
| | Crystallised MI | 12 ± 6 to 194 ± 51 | *This study* |
| **15016** | | | |
| | Homogenised MI | 12 ± 2 to 30 ± 6 | Ni et al. (2019) |
| | Crystallised MI | 18 ± 4 | Ni et al. (2019) |
| | Crystallised MI | 2 ± 1 to 135 ± 39 | *This study* |

(1998) have shown that there is no matrix effect associated with hydrogen isotopic measurement in a partially crystallised MI. Moreover, no trend is observed between the PEC percentage of the MI and its δD, which should be expected if PEC had an influence on the δD values. As such, we do not consider PEC to have played a role in any of the trends observed between $H_2O$ and δD values of the lunar MIs investigated here.

The total range of water concentration reported in MIs across the nine Apollo samples span from 2 μg/g to 212 μg/g (Table 3). Also listed are the $H_2O$ contents determined in homogenised as well as unhomogenised (i.e., crystallised) MIs from 10020, 12008, 12040 and 15016 in previous studies (Chen et al., 2015; Singer et al., 2017; Ni et al., 2019). For these four samples, previously reported ranges in water contents for both crystallised and homogenised MIs fit within our measured range of water contents, once PEC corrections have been implemented (Table 3). It is noted that previously reported ranges are narrower than the ranges seen in our dataset. This could indicate some heterogeneity across individual samples. Moreover, lower water contents are generally noted for MIs that were subjected to homogenisation experiments, possibly reflecting a loss of water during homogenisation of smaller MIs (Chen et al., 2013; Ni et al., 2017).

### 4.4. Presence of shrinkage bubble

Theoretically, formation of a bubble after trapping could alter the primordial δD-$H_2O$ systematics as volatiles will preferentially be partitioned in the bubble. As such, the formation of a shrinkage bubble in a suite of MIs with uniform volatile contents can generate a range in δD-$H_2O$ systematics (Moore et al., 2015). In the studied samples however, it is difficult to assess the possible effect of bubble formation as (i) pre-existing bubble(s) could have been removed during sample cutting and polishing, and (ii) no correlation with water content is observed between MI with an apparent bubble at the surface and those with no visible bubble. For instance, MI #4 from sample 12040 contains a shrinkage bubble (Fig. 1) while being one of the most $H_2O$-rich MI measured in this study (i.e., 194 ± 51 μg/g). Other MIs with apparent shrinkage bubble are MI #13 in 10020, MI #9 in 12020, MI #12, #16 and #21 in 12040, MI #2A and #2B. Without better constraints on the presence or absence of a bubble in an individual MI, we can only acknowledge the possibility of potential effects of bubble formation on volatiles in MIs but are unable to evaluate it further.

### 4.5. Diffusional proton loss through the host silicate

Diffusional proton ($H^+$) loss from a MI through its host can happen during ascent and eruption of basaltic melts. Protons diffuse quickly in pyroxene and olivine hosts (Ingrin and Blanchard, 2006), and MI can lose a few wt% $H_2O$ as well as increase its δD value by a few hundreds of parts per mil over a timescale of hours to a day (Danyushevsky et al., 2002; Gaetani et al., 2012; Bucholz and Gaetani, 2013; Chen et al., 2015). Dry MIs carried in a $H_2O$-rich magma (in a magma-mixing scenario) could potentially gain H instead of losing it (Portnyagin et al., 2008; Gaetani et al., 2012; Hartley et al., 2015). Two mechanisms are associated with diffusional $H^+$ loss (Le Voyer et al., 2014; Roskosz et al., 2018): (i) proton-polaron process, where the charge balance during $H^+$ diffusion is compensated via iron oxidation (Kohlstedt and Mackwell, 1998; Demouchy and Mackwell, 2006); (ii) proton-vacancy process, where the charge balance during $H^+$ diffusion is associated with rearrangement of metal vacancies (Mackwell and Kohlstedt, 1990; Kohlstedt and Mackwell, 1998). These $H^+$ diffusion processes form negative trends in δD vs. $H_2O$ diagrams in the case of $H^+$ loss from MI, as protons diffuse quicker than deuterons (i.e., about 13–

18%, Bucholz and Gaetani, 2013). Shaw et al. (2008) listed the following pieces of evidence which would argue against diffusional $H^+$ loss through a MI host: (i) proof of rapid cooling of the melt - i.e., the absence of daughter minerals, a percentage of PEC < 5%, no Mg-Fe zoning at the inclusion rims - and (ii) the absence of correlation between δD, $H_2O$ and MI size (cf. Fig. 8), where smaller MIs can lose $H_2O$ more easily (Hauri, 2002; Bucholz and Gaetani, 2013). The MIs in studied Apollo basalts exhibit features none of which meet the above two criteria: they possess daughter minerals with high percentage of PEC, they have relatively slow cooling rates, they are relatively small (most are < 20 μm in size) and some samples exhibit negative δD-$H_2O$ correlations, which make them good candidates for having been affected by diffusional proton loss. Moreover, protons could be important H-species in reduced lunar melts (Elkins-Tanton and Grove, 2011).

Some MIs from the Apollo 11 high-Ti basalts show a negative $H_2O$-δD trend (Fig. 10A; $R^2 = 0.71$) that could be explained by $H^+$ diffusion out of MIs. We modelled the diffusional $H^+$ loss through a Rayleigh distillation process (eq. (2)), assuming a maximum decoupling between hydrogen and deuterium diffusion coefficients $D_H / D_D$ of 1.41 (i.e., $\sqrt{\frac{m_H}{m_D}}$) for a dilute ideal gas, as Roskosz et al. (2018) obtained a similar experimental value (1.46) by dehydration of an anhydrous silicate melt at 800 °C and Peslier et al. (2019) obtained a fractionation factor of 1.25 to 2 for augites in nakhlites. As such, diffusional H loss fitting curves have thus to be seen as an upper limit for isotopic fractionation in lunar MIs (Fig. 10A – light grey curves).

$$D/H_t = D/H_0 \times f^{\alpha-1} \quad (2)$$

As a starting composition of the melt, we chose a water concentration of 250 μg/g, close to the highest water concentration measured in our Apollo 11 MI (i.e., 212 μg/g in 10058), and a δD value of + 200 ± 100‰, as representative of the weighted average of the $H_2O$-rich MI from 10020 and 10058. This initial Apollo 11 reservoir has a similar δD value to the one estimated from lunar volcanic glasses and MIs of 74220 and 74002 samples (i.e., +187 ± 19‰ (Saal et al., 2013); +274 ± 42‰ (Füri et al., 2017)). A similar Rayleigh distillation process can be modelled to explain the negative trend observed among some of the Apollo 12 MIs starting from a lower δD value (-100‰; Fig. 10B).

### 4.6. Isotopic exchange

Hydrogen isotopic exchange can occur between a melt inclusion and the crystallising magma through the host crystal if the hydrogen isotope composition of water in the parent magma and in the MI differ (Shaw et al., 2008). However, the rate of such exchange is likely to be small compared to other post-eruptive processes, meaning that this signature may not be measurably large and/or is easily overprinted. Nevertheless, Singer et al. (2017) have argued that isotopic exchange did happen between Apollo 12 basaltic magmas and a low-δD reservoir during slow cooling of the basalts. A low-δD reservoir could be the lunar regolith, which is constantly implanted with solar wind hydrogen (Stephant and Robert, 2014; Treiman et al., 2016). In terms of δD-$H_2O$ systematics, this would be seen as a drop towards more negative δD values, at a given $H_2O$ content (Fig. 9).This process is likely to be relevant for the slowly cooled samples 12040 and 15016, as well as for sample 14072 since these three low-Ti basalts recorded low-δD values between ~ -500‰ and ~ -200‰. Similarly, δD of apatites in each of these samples recorded lower δD values compared to other are basalts (Fig. 7).

### 4.7. Shallow degassing prior to entrapment

It has been shown that $H_2O$ degassing from a melt results in a decrease of δD values of the residual melt, leading to a slightly positive δD vs. $H_2O$ trend (Kyser and O'Neil, 1984; Pineau et al., 1998; Hauri, 2002). However, this isotopic fractionation is limited (δD changes ≤ 100‰; Newman et al., 1988; Pineau et al., 1998; Hauri, 2002). Additionally, given the reduced nature of lunar interior, $H_2$ and H would be a more dominant degassing species, making $H_2O$ unlikely to degas from parental melt (Hirschmann et al., 2012; Saal et al., 2013; Sharp et al., 2013; Tartèse et al., 2013; Renggli et al., 2017). As such, $H_2O$ degassing is not considered here.

### 4.8. Exogenous processes

The Moon is devoid of a protective atmosphere and subject to exogenous processes such as solar wind implantation (Keller and McKay, 1997; McCord et al., 2011) and spallation reactions induced by solar and galactic cosmic rays (Merlivat et al., 1976; Saal et al, 2013; Füri et al., 2017). Protons of solar wind can be implanted down to ~200 nm below the surface (Keller and McKay, 1997) and bond to oxygen atoms of silicate grains to form hydroxyl molecules (OH) (Ichimura et al., 2012; Bradley et al., 2014). The solar wind is devoid of deuterium (with a δD of ~ – 1000‰; (Hashizume et al., 2000; Wiens et al., 2004)). Therefore, any mixing of the initial melt with surface material may cause a reduction in the initial δD values and $H_2O$ content (Fig. 9). Implantation of solar wind has been recorded mostly in lunar agglutinates (Liu et al., 2012; Stephant and Robert, 2014). Treiman et al. (2016) proposed that this D-poor surface reservoir can be incorporated and mixed into mare basalt melts either by assimilation of regolith or by vapor transport from regolith heated by the lava flow, also called metasomatism (Rumpf et al., 2013). Indeed, low-Ti mare basalts 12040 and 15016 are both slowly cooled basalts (Walker et al., 1976; Tikoo et al., 2012), and it has been argued that hydrogen assimilation from the underlying regolith could explain the low δD values of their apatite (Treiman et al, 2016; Barnes et al, 2019) compared to "typical" mare basalt apatite that is characterised by elevated D/H ratios (δD > 500‰) (cf. Fig. 7). Alternatively, it has also been argued that low δD values in MIs of basalt 12040 could have resulted from isotopic exchange with a D-poor reservoir enriched in solar wind hydrogen (see Section 4.5 – Singer et al., 2017; Greenwood et al., 2019). Finally, $H_2O$-δD positive trends observed among Apollo 17 lunar volcanic glasses and MI have been assigned to solar wind

mixing with the pyroclastic melt (Füri et al., 2017 and ref. therein). As such, solar wind is considered as a substantial contributor of hydrogen and may be responsible for low-δD values recorded in various lunar samples.

Interestingly, MIs from 12040 and 15016 show a range of $H_2O$-δD values that can be ascribed to mixing with a D-poor and $H_2O$-poor reservoir (Fig. 10C – dashed line). One potential issue that is worth considering relates to the effect of spallation corrections on the δD values of samples that have very long CRE ages, i.e., ~285 Ma and ~ 400 Ma for 12040 and 15016, respectively (note that we used the new D production rate from Füri et al., 2017). Considering the low water content of MIs in 12040 and 15016, the long CRE ages of these samples, and the large uncertainty on the D production rate (Merlivat et al., 1976; Füri et al., 2017), one might suggest that the observed positive $H_2O$-δD trends result from an over-correction of D produced by spallation (Hauri et al., 2017). Here we consider that the δD values of 12040 and 15016 MIs with water concentrations lower than 25 μg/g are unreliable due to their extreme CRE ages. However, high-Al basalt 14072 follows the same trend defined by 12040 and 15016 (Fig. 10C), while having a relatively short CRE age of 21 Ma (York et al., 1972). The maximum D production associated with spallation reactions for 14072 is associated with a shift of δD values by up to 50‰, and it is unlikely that its positive $H_2O$-δD trend is a result of spallation overcorrection.

High-Al basalt 14072 and its paired companion 14053 are the most reduced basalts retrieved from the Moon, demonstrated by the reduction of fayalite in the mesostasis and spinel minerals in the exterior portions of the rock (Taylor et al., 2004). It has been showed from textural evidence that this reduction proceeded continuously with crystallisation (Haggerty, 1977). Several mechanisms are suggested for sub-solidus reduction of lunar basalts (Brett, 1976; El Goresy, 1976), among which is the basalt extrusion over solar wind ($H^+$) saturated regolith. Indeed, most recently, Taylor et al. (2004) proposed that solar wind protons were most likely reducing agents in case of Apollo 14072 and 14053 basalts. As a result, petrogenesis of 12040, 14072 and 15016 have all been linked to solar wind $H^+$, either by incorporation of solar wind-rich regolith, metasomatism or sub-solidus reduction. This is consistent with both the observed MI $H_2O$-δD trends (Fig. 10C) and the low-δD measured in their apatite compared to "typical" mare basalts (cf. Fig. 7).

We model a mixing curve between a D-poor and $H_2O$-poor (1 ppm) reservoir of −500‰ and an initial melt starting with a composition of $H_2O = 250$ μg/g and δD = -200‰, based on the average δD of the MIs containing the highest $H_2O$ content for these three samples (i.e., −218 ± 154‰) (Fig. 10C – dashed line). Interestingly, we can see that 15016 and 14072 have slightly different trends compared to 12040. These discrepancies imply that either melts forming 12040, 14072 and 15016 had different $H_2O$-δD initial composition, or 12040, 14072 and 15016 melts had similar $H_2O$-δD initial composition, but 15016 and 14072 were affected by H diffusion. The same mixing curve can also explain the positive trend observed for Apollo 11 samples, but in this case the starting composition for δD = +200‰ (also based on the average of δD from the $H_2O$-rich MI from 10020 and 10058), as defined for diffusional $H^+$ loss (Fig. 10A).

## 5. IMPLICATIONS FOR THE MOON

### 5.1. Estimation of the water content of the mare-basalt parental magmas

A common practice while studying the $H_2O$ content of MIs is to take the highest reported $H_2O$ to represent the pre-degassing $H_2O$ content of the melt (Saal et al., 2008; Hauri et al., 2011; Chen et al., 2015). However, an early-formed MI should contain less water than a later-formed MI as the melt gets enriched in $H_2O$ during fractional crystallisation, if no other process is involved. The variability in water contents of Apollo 12 MIs appears to be mainly controlled by fractional crystallisation (cf. Fig. 8), with few exceptions where H diffusion is also involved. As such, the MI entrapped in highest Mg# host should be the better proxy for estimating volatile signature of the parental melt. Based on the four MIs in Apollo 12 basalts that are hosted in silicates with Mg# > 70 (excluding MIs showing high H isotopic fractionation), we estimate an initial water content of the parental melt for Apollo 12 suite to be 10 ± 4 μg/g $H_2O$. Interestingly, 12040 crystallised from a more evolved melt, as revealed by the lower Mg# of MI hosts. This observation is consistent with relatively $H_2O$-rich nature of MIs in 12040 compared to the other samples from the Apollo 12 suite. The naturally glassy MI #4A is probably the most pristine MI in this sample and recorded the highest water content for this sample at 194 ± 51 μg/g $H_2O$.

Because other samples do not show any correlation between the water content in MI and their hosts' Mg#, we chose to use their highest water content (PEC corrected) as lower limit of the pre-eruptive abundance of their magma. Samples 14072 and 15016 are similar to 12040 in term of $H_2O$-δD systematics of both MIs and apatites (Fig. 10C). Their highest MI water contents are 73 ± 44 and 135 ± 39 μg/g $H_2O$, respectively. Finally, Apollo 11 samples 10020 and 10058 showed higher water contents in the early-formed MIs, i.e., 161 ± 65 and 212 ± 27 μg/g $H_2O$. One should note here that we decide to report $H^-/^{18}O^-$ ratios measured in lunar MI into equivalent $H_2O$ concentrations, and therefore, it is possible that we might have overestimated $H_2O$ concentrations in the parent melts as some H might be speciated under other H forms. As such, these values should be seen as upper limits.

Water contents thus seem to be heterogeneous among mare parental magmas. While Apollo 10020, 10058, 12040, 14072 and 15016 parental magmas appears to have broadly similar range for their water contents (100–200 μg/g $H_2O$), the Apollo 12 suite is highly depleted in water, with an estimated average of 10 μg/g $H_2O$ for the parental magmas. Assuming a range between 3 and 30% partial melting in the lunar mantle (Binder, 1982; Shearer and Papike, 1993; Hallis et al., 2014), we estimate a water content for the source region of most Apollo basalts studied

here in the region of 3–60 μg/g $H_2O$, and lower than 3 μg/g $H_2O$ for the Apollo 12 samples.

This lunar mantle water concentration estimate of ~3 to 60 μg/g $H_2O$ is towards the lower range of estimates based on various lunar phases. Apatite from mare and KREEP-basalts tends to be water-rich (Boyce et al., 2010; McCubbin et al., 2010b; Greenwood et al., 2011; Tartèse et al., 2013, 2014) and the water content for their source regions has been estimated to be between 0.64 and 450 μg/g $H_2O$ (McCubbin et al., 2010b; Tartèse et al., 2013), calculated for 3 and 30% partial melting of the lunar mantle. However, these estimates based on apatite volatile abundances need to be taken with caution (e.g., Boyce et al., 2014). Indeed, McCubbin et al. (2015) revised their previous estimate to 0.15 to 5.3 μg/g $H_2O$, arguing that higher estimates are biased towards wettest samples. Based on 74220 lunar volcanic glasses and their MIs, Hauri et al. (2011) estimated a water content for the lunar mantle of between 79 and 409 μg/g $H_2O$ (calculated for 5 and 30% partial melting, resp.). This range was later revised between 133 and 292 μg/g $H_2O$ (Hauri et al., 2015) based on ratios of volatile to non-volatile elements in Apollo 15 and 17 pyroclastic glasses (Saal et al., 2008). Despite the fact that the high-water concentration of the 74220 parental melt (~1410 μg/g $H_2O$) has been considered by some as a local anomaly (Albarede et al., 2015), the similarity between the volatile/refractory element ratios for MIs from 74220 and for MIs, glass beads, and mare basalts from other lunar samples suggests the opposite (Ni et al., 2019), indicating that these pyroclastic deposits are one of the best proxies to ascertain lunar mantle volatile concentrations. Füri et al. (2014) estimated a water concentration from 74002 LVG in the lower range of 74220 estimation, i.e., between 4 and 92 μg/g $H_2O$ (for 3 and 30% partial melting, resp.). Similar to Hauri et al. (2015), Chen et al. (2015) estimated a lunar mantle with $111 \pm 23$ μg/g $H_2O$ from mare basalt MI study, while Ni et al. (2019) estimated ~84 μg/g $H_2O$. Singer et al. (2017) also measured 740 μg/g $H_2O$ in 12018 mare basalt MIs (Fig. 6), which can be converted into ~25–160 μg/g $H_2O$ for its source region. All these sample-based estimates of bulk lunar mantle appear higher, with the exception of McCubbin et al. (2015) estimate (i.e., 0.15 to 5.3 μg/g $H_2O$), than the estimate of Elkins-Tanton and Grove (2011) of <10 μg/g $H_2O$ for the bulk lunar interior, which they derived from petrological and magma ocean modelling.

The relatively long cooling time, i.e., weeks to years, of mare basalts (Holness et al., 2012) compared to volcanic glasses, i.e., minutes, is the best explanation for the preservation of higher water concentration in Apollo 17 LVG and MIs (e.g., up to ~1410 μg/g; Hauri et al., 2015) compared to other lunar basaltic samples (e.g., Chen et al., 2015; Ni et al., 2019). Indeed, crystallised MIs may have undergone loss of hydrogen, either by trapping of a degassed melt, or during post-entrapment H diffusion. Similarly, apatite likely crystallised after intense H degassing from mare magmas (Greenwood et al., 2011; Tartèse and Anand, 2013; Tartèse et al., 2013). As such, our estimates of water concentration in mare source regions are likely to be towards the lower end of the actual range.

A lunar mantle water concentration of ~3–60 μg/g $H_2O$ might seem high when considering (i) modelling of the crystallisation of the LMO that suggests a concentration of ~10 ppm $H_2O$ (Elkins-Tanton and Grove, 2011), and (ii) the difficulty in water retention during the high-energy formation event of the Moon and the expected hydrodynamic escape of volatiles (Pahlevan and Stevenson, 2007; Canup, 2012). Hauri et al. (2015) suggested that either the Moon inherited its water solely from the Earth, or that only 25% of the water originated from proto Earth-derived material and the remaining came from highly degassed material from the protolunar disk. Recent studies show that indigenous lunar water may indeed be a complement of terrestrial water that survived the high-energy lunar formation event (Greenwood et al., 2018), along with some water that was delivered by carbonaceous chondrite-like material during late accretion (Tartèse and Anand, 2013; Barnes et al., 2016; Hauri et al., 2017).

### 5.2. Unravelling H isotope composition of the primordial lunar water

#### *5.2.1. Multiple processes modifying MI hydrogen signature in lunar basalts*

Melt inclusions in nominally anhydrous minerals are supposedly a good proxy to document the variety of magmatic and secondary processes that have affected their volatile inventory (Danyushevsky et al., 2002; Hauri, 2002; Massare et al., 2002; Severs et al., 2007; Steele-MacInnis et al., 2011; Gaetani et al., 2012; Bucholz and Gaetani, 2013). Lunar basaltic MIs have undergone $H^+$ diffusion, and their parent melts experienced interaction with a D-poor reservoir (probably as a result of solar wind-rich regolith incorporation) prior to entrapment in MIs. Analyses of several (>5) MIs in a single sample is thus required in order to identify δD-$H_2O$ trends and the associated process (es) to unravel the initial magmatic δD-$H_2O$ values.

Melt inclusions in 10020 and 10058 high-Ti basalts show evidence of diffusional proton loss as well as evidence of mixing with a D-poor $H_2O$-poor reservoir, for which the initial value could have been as low as −500‰. The parental melts of these two samples could have interacted with solar wind-rich regolith either by incorporation, metasomatism or sub-solidus reduction, as suggested for samples 12040, 14072 and 15016 (Taylor et al., 2004; Treiman et al., 2016; Barnes et al, in press). From modelling of these two processes (Fig. 10A), we estimated that the source-region water reservoir of these two samples had a δD of $\sim +200 \pm 100$‰, even though these two samples represent separate igneous cooling units (Beaty and Albee, 1978). Interestingly, apatite from both 10058 and 10020 are in disequilibrium with this initial value, with average δD values of ~ +800‰ for 10058 apatite (Tartèse et al., 2013) and +600‰ for 10020 apatite (Fig. 7). This suggests that apatite in 10058 and 10020 crystallised after significant $H_2$ degassing after entrapment of MIs (e.g., Tartèse et al., 2013).

The Apollo 12 basalt suite (excluding sample 12040) documents a different story. All of these basalts (i.e., 12002, 12004, 12008 and 12020) are relatively rapidly cooled (>1C/h - Walker 1976). Their parental melts seem

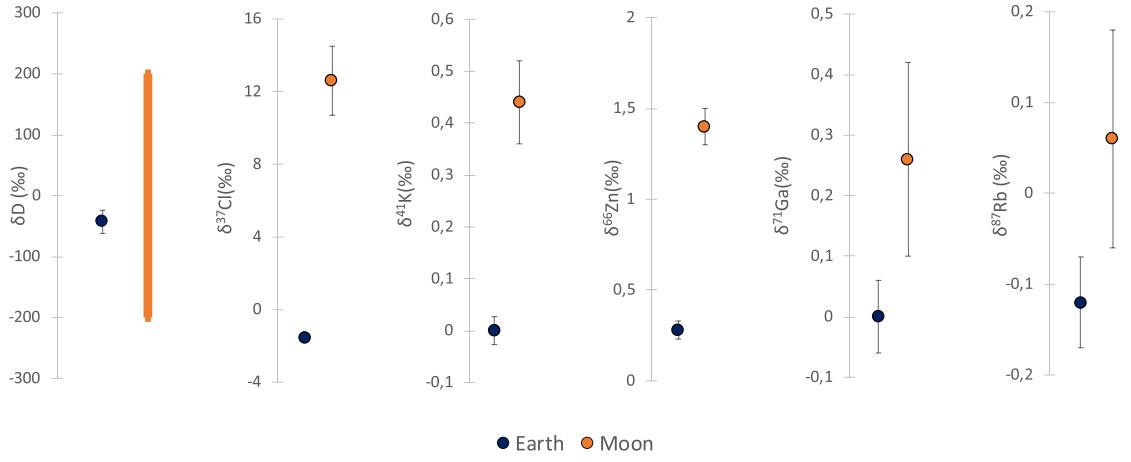


Fig. 11. Isotopic composition of volatile elements (in permil) for the bulk-silicate Earth compared to the Moon. Hydrogen isotopic values are from Lécuyer et al. 1998 and this study, for Earth and Moon, respectively; chlorine isotopic composition are from Bonifacie et al (2008) and Stephant et al. (2019), respectively; potassium isotopic composition from Wang and Jacobsen (2016); zinc isotopic composition from Day and Moynier (2014) and references therein; gallium isotopic composition from Kato and Moynier (2017); rubidium isotopic composition from Pringle and Moynier (2017).

to have been unaffected by magmatic and secondary processes. Water content in the MIs is dependent on the timing of MI entrapment. Considering all MIs located in silicates with Mg# > 70, the δD value for the parental melt of Apollo 12 suite is estimated to be −157 ± 65‰, lower than what is estimated for Apollo 11 high-Ti basalts. This estimation is consistent with 12018 MIs previously measured with water contents up to 740 ± 74 μg/g. The δD values of apatite in Apollo 12002 and 12004 basalts are >500‰ (cf. Fig. 7). This is typical of mare basalt apatite, suggesting that these samples have undergone severe $H_2$ degassing prior to apatite formation, explaining this large discrepancy between MIs and apatite D/H ratios.

For samples 12040, 15016 and 14072, the only process that seems to have altered the initial δD-$H_2O$ signal is mixing with solar wind-implanted material. In these samples, the limited variation between δD values of MIs and apatite reveals that apatite are close to equilibrium with the melt, with δD values of apatite ranging between −200 and +200‰ for 12040 (Greenwood et al., 2011; Boyce et al., 2015; Singer et al., 2017; this study), between −100 and +500‰ for 15016 (Barnes et al, in press) and between 0 and +400‰ for 14072 (this study – cf. Fig. 7). These three samples thus seem to record a different volatile history than other mare basalts: their parent melts may have been affected by magmatic degassing of H-bearing species to a lesser extent than "typical" mare basalts, later overprinted by mixing with a solar wind-rich component, either by incorporation of solar wind-rich regolith material (Treiman et al., 2016), metasomatism (Rumpf et al., 2013; Potts et al., 2018) or due to sub-solidus reduction of the basalt (Haggerty, 1977; Taylor et al., 2004). Mare basalts 12040 and 15016 are both slowly cooled samples compared to other typical mare basalts (Walker et al., 1976; Tikoo et al., 2012). Singer et al. (2017) have interpreted the lower water abundance in slowly cooled sample 12040 as suggesting that slow cooling favour degassing. We do not see evidence suggesting that 12040 was affected by larger extent of $H_2O$ or $H_2$ degassing in our dataset compared to data for more rapidly-cooled samples. Based on both the δD values of MIs with the highest water concentration in these samples and our solar wind implantation model, the δD of 12040, 15016 and 14072 initial reservoirs are estimated to be ∼ −200‰.

Apollo 11 high-Ti basalts 10020 and 10058, Apollo 12 low-Ti basalts 12002, 12004, 12008, 12020 and 12040, Apollo 14 high-Al basalt 14072 and Apollo 15 low-Ti basalt 15016 were derived from distinct parental melts, due to the heterogeneity of the lunar mantle at the time of generation of mare magmas (Hallis et al, 2014). As revealed by the $H_2O$-δD systematics of their MIs, each of these parental melts also had different initial δD values, ranging between −200‰ and +200‰. Our findings are therefore consistent with the present understanding that the water in the Moon has a broadly chondritic origin (Saal et al., 2013; Tartèse and Anand, 2013; Barnes et al., 2016).

### 5.2.2. Origin of the lunar hydrogen – a conundrum?

The inferred hydrogen isotopic composition for the lunar interior (i.e., −200 to +200‰) does not seem significantly higher compared to that of the Earth's mantle (i.e., −43 ± 19‰; Lécuyer et al., 1998). This appears to be in contrast with the isotopic signatures of lunar samples for moderately volatile elements such as chlorine (Sharp et al., 2010; Tartèse et al., 2014; Treiman et al., 2014; Boyce et al., 2015; Barnes et al., 2016; Potts et al., 2018; Stephant et al., 2019; Wang et al., 2019), zinc (Moynier et al., 2006; Paniello et al., 2012; Kato et al., 2015), rubid-

ium (Pringle and Moynier, 2017), potassium (Wang and Jacobsen, 2016) and gallium (Kato and Moynier, 2017) (Fig. 11). However, heavier isotopic composition compared to the Earth for these volatiles and moderately volatile elements for the Moon are consistent with volatile loss of these elements either during the giant impact (Paniello et al., 2012; Wang and Jacobsen, 2016) or during the LMO differentiation (Day and Moynier, 2014; Kato et al., 2015; Barnes et al., 2016). At face value, lunar hydrogen isotopes are thus difficult to reconcile with existing lunar formation scenarios unless (i) the initial δD signature of indigenous lunar water was lighter than carbonaceous chondrite-like D/H values and increased because of $H_2$ degassing from the LMO (Desch and Robinson, 2019), or, more likely, (ii) much of the lunar water was added late, after the main phase of LMO solidification, by carbonaceous-chondrite like material. This water was subsequently sampled by the younger mare basalts and pyroclastic deposits (Tartèse and Anand, 2013; Barnes et al., 2016; Hauri et al., 2017).

## 6. CONCLUSION

The abundance and origin of water in the lunar interior is crucial for our understanding of the Moon's formation and magmatic differentiation processes. However, lunar samples have been affected by various magmatic and secondary processes that make estimating the initial $H_2O$-δD systematics of basaltic parental melts challenging. In this study we have measured $H^-/^{18}O^-$ ratio (reported in terms of equivalent $H_2O$ concentration) and the H isotopic composition of 56 olivine- and pyroxene-hosted MIs, and 13 apatites, from nine different mare basalts collected by four Apollo missions. Melt inclusions from mare basalts reveal that several magmatic and secondary processes have affected their original $H_2O$ contents and δD values, as well as that of their parental magmas. These processes include crystallisation, diffusional proton loss through the silicate hosts (olivine and pyroxene), mixing of solar wind-derived and indigenous water reservoirs, metasomatism, and sub-solidus reduction. Based on modelling for the effects of all these processes on our dataset of studied mare basalts, we estimate initial water abundances of ~10 μg/g $H_2O$ for parental magmas of Apollo 12 basaltic suite while between 100 and 200 μg/g $H_2O$ for Apollo 11 samples, and samples 12040, 14072 and 15016. Furthermore, the δD values of these basaltic parent melts (and that of their mantle source regions) ranged between −200‰ to +200‰, concordant with the hypothesis of a carbonaceous chondrite-like hydrogen isotopic signature for indigenous lunar water. This study highlights the fact that MIs are not a closed system with respect to hydrogen gain and/or loss and associated hydrogen isotope fractionation processes. However, they remain a good proxy to disentangle various magmatic and secondary processes as long as several (>5) MIs are analysed in each studied sample. If possible, future studies should focus on samples with relatively short CRE ages to reduce the considerable uncertainties in determining the primary H isotopic signature of lunar water.

## Declaration of Competing Interest

The authors declare that they have no known competing financial interests or personal relationships that could have appeared to influence the work reported in this paper.

### ACKNOWLEDGEMENTS

We thank NASA CAPTEM for allocation of Apollo samples. We thank Marc Norman, Youxue Zhang and two anonymous reviewers for their very detailed but constructive comments all of which helped improve the quality of this manuscript substantially. This research was supported by a STFC grant to MA and IAF (grant #ST/P000657/1). RT acknowledges STFC for financial support (grant #ST/P005225/1).

## APPENDIX A. SUPPLEMENTARY MATERIAL

Supplementary data to this article can be found online at https://doi.org/10.1016/j.gca.2020.06.017.

## REFERENCES

Albarede F., Albalat E. and Lee C.-T.-A. (2015) An intrinsic volatility scale relevant to the Earth and Moon and the status of water in the Moon. *Meteorit. Planet. Sci.* **50**(4), 568–577.

Alexander E. C. (1971) Spallogenic Ne, Kr, and Xe from a depth study of 12002. In *Proc. Lunar Sci. Conf.*, pp. 1643–1650.

Anand M. (2010) Lunar water: a brief review. *Earth Moon Planets*. https://doi.org/10.1007/s11038-010-9377-9.

Aubaud C., Withers A., Hirschmann M., Guan Y., Leshin Y., Mackwell S. and Bell D. (2007) Intercalibration of FTIR and SIMS for hydrogen measurements in glasses and nominally anhydrous minerals. *Am. Mineral.* **92**, 811–828.

Barnes J. J., Franchi I. A., Anand M., Tartèse R., Starkey N. A., Koike M., Sano Y. and Russell S. S. (2013) Accurate and precise measurements of the D/H ratio and hydroxyl content in lunar apatites using. NanoSIMS. *Chem. Geol.* **337–338**, 48–55.

Barnes J. J. et al. (2014) The origin of water in the primitive Moon as revealed by the lunar highlands samples. *Earth Planet. Sci. Lett.* **390**, 244–252.

Barnes J. J., Tartèse R., Anand M., McCubbin F. M., Neale C. R. and Franchi I. A. (2016) Early degassing of lunar urKREEP by crust-breaching impact(s). *Earth Planet. Sci. Lett.* **447**, 84–94.

Barnes J. J., Franchi I. A., McCubbin F. M. and Anand M. (in press) Multiple volatile reservoirs in the lunar interior revealed by the isotopic composition of chlorine in lunar basalts. *Geochim. Cosmochim. Acta.* **206**, 144–162. https://doi.org/10.1016/j.gca.2018.12.032.

Beaty D. W. and Albee A. L. (1978) Comparative petrology and possible genetic relations among Apollo 11 basalts. In *Proceedings of the 9th Lunar and Planetary Science Conference*, pp. 359–463.

Bindeman I. N., Kamenetsky V. S., Palandri J. and Vennemann T. (2012) Hydrogen and oxygen isotope behaviors during variable degrees of upper mantle melting: Example from the basaltic glasses from Macquarie Island. *Chem. Geol.* **310–311**, 126–136.

Binder A. B. (1982) The mare basalt magma source region and mare basalt magma genesis. *J. Geophys. Res.* **87**, A37–A53. https://doi.org/10.1029/JB087iS01p00A37.

Bradley J. P., Ishii H. A., Gillis-Davis J. J., Ciston J., Nielsen M. H., Bechtel H. A. and Martin M. C. (2014) Detection of solar

wind-produced water in irradiated rims on silicate minerals. *Proc. Natl. Acad. Sci.* **111**(5), 1732–1735.

Brett R. (1976) Reduction of mare basalts by sulfur loss. *Geochim. Cosmo. Acta* **40**, 997–1004.

Bogard D. D., Funkhouser J. G., Schaeffer O. A. and Zahringer J. (1971) Noble gas abundances in lunar material-cosmic ray spallation products and radiation ages from the Sea of Tranquility and the Ocean of Storms. *J. Geophys. Res.* **76**, 2757–2779.

Bombardieri D. J., Norman M. D., Kamenetsky V. S. and Danyushevsky L. V. (2005) Major element and primary sulfur concentrations in Apollo 12 mare basalts: the view from melt inclusions. *Meteorit. Planet. Sci.* **40**(5), 679–693.

Bonifacie M., Jendrzejewski N., Agrinier P., Humler E., Coleman M. and Javoy M. (2008) The chlorine isotope composition of the Earth's mantle. *Science* **319**, 1518–1520.

Boyce J. W. et al. (2010) Lunar apatite with terrestrial volatile abundances. *Nature* **466**, 466–469.

Boyce J. W., Tomlinson S. M., McCubbin F. M., Greenwood J. P. and Treiman A. H. (2014) The Lunar Apatite Paradox. Science Express.

Boyce J. W., Treiman A. H., Guan Y., Ma C., Eiler J. M., Gross J., Greenwood J. P. and Stolper E. M. (2015) The chlorine isotope fingerprint of the lunar magma ocean. *Sci. Adv.* **1**(8).

Bucholz C. E., Gaetani G. A., Behn M. D. and Shimizu N. (2013) Post-entrapment modification of volatiles and oxygen fugacity in olivine-hosted melt inclusions. *Earth Planet. Sci. Lett.* **374**, 145–155.

Burnett D. S., Drozd R. J., Morgan C. J. and Pososek F. A. (1975) Exposure histories of Bench crater rocks. *Proc. Lunar Sci. Conf.* **6th**, 2219–2240.

Cannatelli C., Doherty A. L., Esposito R., Lima A. and De Vivo B. (2016) Understanding a volcano through a droplet: a melt inclusion approach. *J. Geochem. Explor.* **171**, 4–19.

Canup R. M. (2012) Forming a Moon with an Earth-like composition via a giant impact. *Science*, 10.1126.2012/science.1226073.

Chen Y., Provost A., Schiano P. and Cluzel N. (2013) Magma ascent rate and initial water concentration inferred from diffusive water loss from olivine-hosted melt inclusions. *Contrib. Mineral. Petrol.* **165**, 525–541.

Chen Y., Zhang Y., Liu Y., Guan Y., Eiler J. and Stolper E. M. (2015) Water, fluorine, and sulfur concentrations in the lunar mantle. *Earth Planet. Sci. Lett.* **427**, 37–46.

Dalou C., Hirschmann M. M., Jacobsen S. D. and Le Losq C. (2019) Raman spectroscopy study of C-O-H-N speciation in reduced basaltic glasses: Implications for reduced planetary mantles. *Geochim. Cosmo. Acta* **265**, 32–47.

Danyushevsky L. V., McNeill A. W. and Sobolev A. V. (2002) Experimental and petrological studies of melt inclusions in phenocrysts from mantle-derived magmas: an overview of techniques, advantages and complications. *Chem. Geol.* **183**, 5–24.

Danyushevsky L. V. and Plechov P. (2011) Petrolog3: integrated software for modelling crystallization processes. *Geochem. Geophys. Geosyst.* **12**, 7.

Day M. D. and Moynier F. (2014) Evaporative fractionation of volatile stable isotopes and their bearing on the origin of the Moon. *Philos. Trans. R. Soc.* **A372**, 20130259.

Demouchy S. and Mackwell S. (2006) Mechanisms of hydrogen incorporation and diffusion in iron-bearing olivine. *Phys. Chem. Miner.* **33**, 347–355.

Desch S. J. and Robinson K. L. (2019) A unified model for hydrogen in Earth and Moon: No one expects the Theia contribution. *Geochemistry* **79** 125546.

El Goresy, A. 1976. Oxide minerals in lunar rocks. In Oxide Minerals. Min. Soc. Amer. Short Course Notes (S. Rumble III, ed.), 3, 1–46.

Elkins-Tanton L. T. and Grove T. L. (2011) Water (hydrogen) in the lunar mantle: Results from petrology and magma ocean modeling. *Earth Planet. Sci. Lett.* **307**(1a2), 173–179.

Esposito R., Klebesz R., Bartoli O., Klyukin Y. I., Moncada D., Doherty A. L. and Bodnar R. J. (2012) Application of the Linkam TS1400XY heating stage to melt inclusion studies. *Cent. Eur. J. Geosci.* **4**(2), 208–218.

Füri E., Deloule E., Gurenko A. and Marty B. (2014) New evidence for chondritic lunar water from combined D/H and noble gas analyses of single Apollo 17 volcanic glasses. *Icarus* **229**, 109–120.

Füri E., Deloule E. and Trappitsch R. (2017) The production rate of cosmogenic deuterium at the Moon's surface. *Earth Planet. Sci. Lett.* **474**, 76–82.

Gaetani G. A., O'Leary J. A., Shimizu N., Bucholz C. E. and Newville M. (2012) Rapid reequilibration of H2O and oxygen fugacity in olivine-hosted melt inclusions. *Geology* **40**(10), 915–918.

Geiss J. and Gloecker G. (1998) Abundances of Deuterium and Helium-3 in the protosolar cloud. *Space Sci. Rev.* **84**, 239–250.

Giesting P. A., Schwenzer S. P., Filiberto J., Starkey N. A., Franchi I. A., Treiman A. H., Tindle A. G. and Grady M. M. (2015) Igneous and shock processes affecting chassignite amphibole evaluated using chlorine/water partitioning and hydrogen isotopes. *Meteorit. Planet. Sci.* **50**, 433–460.

Goldoff B., Webster J. D. and Harlow D. E. (2012) Characterization of fluor-chlorapatites by electron probe microanalysis with a focus on time-dependent intensity variation of halogens. *Am. Mineral.* **97**, 1103–1115.

Gonfiantini R. (1978) Standards for stable isotope measurements in natural compounds. *Nature* **271**, 534–536.

Greenwood J. P. et al. (2011) Hydrogen isotope ratios in lunar rocks indicate delivery of cometary water to the Moon. *Nature Geosci.* **4**, 79–82.

Greenwood J. P., Itoh S., Kawasaki N., Sakamoto N. and Yurimoto H. (2019) Hydrogen isotopes, volatile, and refractory trace element composition of melt inclusions and apatite in a consanguineous suite of Apollo 12 olivine basalts. *Lunar and Planetary Science Conference 50th. Abst #2371*.

Greenwood R. C., Barrat J. A., Miller M. F., Anand M., Dauphas N., Franchi I. A., Sillard P. and Starkey N. A. (2018) Oxygen isotopic evidence for accretion of Earth's water before a high-energy Moon-forming giant impact. *Sci. Adv.* **4**, 3. https://doi.org/10.1126/sciadv.aao5928.

Grewal D. S., Dasgupta R. and Farnell A. (2020) The speciation of carbon, nitrogen, and water in magma oceans and its effect on volatile partitioning between major reservoirs of the Solar System rocky bodies. *Geochim. Cosmochim. Acta* **280**, 281–301.

Guggisberg S., Eberhardt P., Geiss J., Grogler N., Stettler A., Brown G. M. and Pecket A. (1979) Classification of the Apollo-11 basalts according to Ar39-Ar40 ages and petrological properties. In *Proc. 10th Lunar Planet. Sci. Conf*, pp. 1–39.

Hagemann F., Nief G. and Roth E. (1970) Absolute isotopic scale for deuterium analyses of natural waters. Absolute D/H ratio for SMOW. *Tellus* **22**(6), 712–715.

Haggerty S. E. (1977) Apollo 14: Oxide, metal and olivine mineral chemistries 14072 with a bearing on the temporal relationship with subsolidus reduction. In *Proc. Lunar Conf. 8th*, pp. 1809–1829.

Halliday A. N. (2013) The origin of volatiles in the terrestrial planets. *Geochim. Cosmochim. Acta* **105**, 146–171.

Hallis L. J., Anand M. and Strekopytov S. (2014) Trace-element modelling of mare basalt parental melts: implications for a

heterogeneous lunar mantle. *Geochim. Cosmochim. Acta* **134**, 289–316.
Hartley M. E., Neave D. A., Maclennan J., Edmonds M. and Thordarson T. (2015) Diffusive over-hydration of olivine-hosted melt inclusions. *Earth Planet. Sci. Lett.* **425**, 168–178.
Hashizume K., Chaussidon M., Marty B. and Robert F. (2000) Solar wind record on the Moon: Deciphering presolar from planetary nitrogen. *Science* **290**, 1142–1145.
Hauri E. H., Wang J., Dixon J. E., King P. L., Mandeville C. and Newman S. (2002a) SIMS analysis of volatiles in silicate glasses: 1. Calibration, matrix effects and comparisons with FTIR. *Chem. Geol.* **183**(1–4), 99–114.
Hauri E. (2002) SIMS analysis of volatiles in silicate glasses, 2: isotopes and abundances in Hawaiian melt inclusions. *Chem. Geol.* **183**, 115–141.
Hauri E. H., Weinreich T., Saal A. E., Rutherford M. C. and Van Orman J. A. (2011) High pre-eruptive water contents preserved in lunar melt inclusions. *Science* **333**, 213–215.
Hauri E. H., Saal A. E., Rutherford M. C. and Van Orman J. A. (2015) Water in the Moon's interior: truth and consequences. *Earth Planet. Sci. Lett.* **409**, 252–264.
Hauri E. H., Saal A. E., Nakajima M., Anand M., Rutherford M. C., Van Orman J. A. and Le Voyer M. (2017) Origin and evolution of water in the moon's interior. *Annu. Rev. Earth Planet. Sci.* **45**, 89–111.
Hintenberger H., Weber H. W. and Takaoka N. (1971) Concentrations and isotopic abundances of the rare gases in lunar matter. In *Proc. Lunar Sci. Conf.*, pp. 1607–1625.
Hirschmann M. M., Withers A. C., Ardia P. and Foley N. T. (2012) Solubility of molecular hydrogen in silicate melts and consequences for volatile evolution of terrestrial planets. *Earth and Planetary Science Letters* **345–348**, 38–48.
Holloway J. R., and Blank J. G. (1994) Application of experimental results to C-O-H species in natural melts. In Volatiles in magmas. Rev. Min. (eds. M.R. Carroll and J.R. Holloway), vol. 30, 187–230.
Holness M. B., Richardson B. and Anand M. (2012) A new proxy for dolerite crystallisation times in planetary samples. *43rd Lunar and Planetary Science Conference, Abstract #1589*.
Hui H., Peslier A., Zhang Y. and Neal C. R. (2013) Water in lunar anorthosites and evidence for a wet early Moon. *Nature Geosci.* **6**, 177–180.
Hui H., Guan Y., Chen Y., Peslier A. H., Zhang Y., Liu Y., Flemming R. L., Rossman G. R., Eiler J. M., Neal C. R. and Osinski G. R. (2017) A heterogeneous lunar interior for hydrogen isotopes as revealed by the lunar highlands samples. *Earth Planet. Sci. Lett.* **473**, 14–23.
Ichimura A. S., Zent A. P., Quinn R. C., Sanchez M. R. and Taylor L. A. (2012) Hydroxyl (OH) production on airless planetary bodies: evidence from H+/D+ ion-beam experiments. *Earth Planet. Sci. Lett.* **345–348**, 90–94.
Ingrin J. and Blanchard M. (2006) Diffusion of hydrogen in minerals. *Rev. Mineral. Geochem.* **62**, 291–320.
Kato C., Moynier F., Valdes M. C., Dhaliwal J. K. and Day J. M. D. (2015) Extensive volatile loss during formation and differentiation of the Moon. *Nat. Commun.* **6**, 7617.
Kato C. and Moynier F. (2017) Gallium isotopic evidence for extensive volatile loss from the Moon during its formation. *Sci. Adv.* **6**, 7617.
Kent A. J. R. (2008) Melt inclusions in basaltics and related volcanic rocks. *Review in Mineralogy and Geochemistry* **69**, 273–331.
Keller L. P. and McKay D. S. (1997) The nature and origin of rims on lunar soil grains. *Geochim. Cosmochim. Acta* **61**(11), 2331–2341.
Klein C., Drake J. C. and Frondel C. (1971) Mineralogical, petrological, and chemical features of four Apollo 12 lunar microgabbros. In *Proc. 2nd Lunar Sci. Conf.*, pp. 265–284.
Kohlstedt D. L. and Mackwell S. J. (1998) Diffusion of hydrogen and intrinsic point defects in olivine. *Z. Phys. Chem.* **207**, 147–162.
Koga K, Hauri E.H., Hirschmann M., Bell D. Hydrogen concetration analyses using SIMS and FTIR: comparisons and calibration for nominally anhydrous minerals. Geochemistry Geophysics Geosystems, 4, 2003.
Kushiro I. and Haramura H. (1971) Major element variation and possible source materials of Apollo 12 crystalline rocks. *Science* **171**, 1235–1237.
Kyser T. K. and O'Neil J. R. (1984) Hydrogen isotope systematics of submarine basalts. *Geochim. Cosmochim. Acta* **48**, 2123–2133.
Le Voyer M., Asimow P. D., Mosenfelder J. L., Guan Y., Wallace P. J., Schiano P., Stolper E. M. and Eiler J. M. (2014) Zonation of H2O and F concentrations around melt inclusions in olivines. *J. Petrol.* **55**(4), 685–707.
Lécuyer C., Gillet P. and Robert F. (1998) The hydrogen isotope composition of seawater and the global water cycle. *Chem. Geol.* **145**(3-4), 249–261.
Liu Y., Guan Y., Zhang Y., Rossman G. R., Eiler J. M. and Taylor L. A. (2012) Direct measurement of hydroxyl in the lunar regolith and the origin of lunar surface water. *Nat. Geosci.* **5** (11), 779–782. https://doi.org/10.1038/ngeo1601.
Lowenstern J. B. (2003) Melt inclusions come of age: volatiles, volcanoes, and sorby's legacy. *Develop. Volcanol.* **5**, 1–21.
Mackwell S. J. and Kohlstedt D. L. (1990) Diffusion of hydrogen in olivine: implications for water in the mantle. *J. Geophys. Res.* **95**, 5079–5088.
Marty B. (2012) The origins and concentrations of water, carbon, nitrogen and noble gases on Earth. In *Earth Planet. Sci. Lett.*, 313–314, pp. 56–66. Earth Planet. Sci. Lett..
Massare D., Métrich N. and Clocchiatti R. (2002) High-temperature experiments on silicate melt inclusions in olivine at 1 atm: inference on temperatures of homogenization and H2O concentrations. *Chem. Geol.* **183**, 87–98.
Maxwell J. A. and Wiik H. B. (1971) Chemical composition of Apollo 12 lunar samples 12004, 12033, 12051, 12052 and 12065. *Earth Planet. Sci. Lett.* **10**, 285–288.
McCord T. B., Taylor L. A., Combe J. P., Kramer G., Pieters C. M., Sunshine J. M. and Clark R. N. (2011) Sources and physical processes responsible for OH/H2O in the lunar soil as revealed by the Moon Mineralogy Mapper (M3). *J. Geophys. Res. Planets* **116**(E6), E00G05.
McCubbin F. M. et al. (2011) Fluorine and chlorine abundances in lunar apatite: implications for heterogeneous distributions of magmatic volatiles in the lunar interior. *Geochim. Cosmochim. Acta* **75**, 5073–5093.
McCubbin F. M. et al. (2010a) Detection of structurally bound hydroxyl in apatite from Apollo mare basalt 15058,128 using TOF-SIMS. *Am. Mineral.* **9**, 1141–1150.
McCubbin F. M. et al. (2010b) Nominally hydrous magmatism on the Moon. *Proc. Natl Acad. Sci. USA* **107**, 11223–11228.
McCubbin F. M., Hauri E. H., Elardo S. M., Vander Kaaden K. E. and Wang J. (2012) Hydrous melting of the martian mantleproduced both depleted and enriched shergottites. *Geology* **40**, 683–686.
McCubbin F. M., Vander Kaaden K. E., Tartèse R., Klima R. L., Liu Y., Mortimer J., Barnes J. J., Shearer C. K., Treiman A. H., Lawrence D. J., Elardo S. M., Hurley D. M., Boyce J. W. and Anand M. (2015) Magmatic volatiles (H, C, N, F, S, Cl) in the lunar mantle, crust, and regolith: Abundances, distributions,

processes, and reservoirs. *American Mineralogist* **100**, 1668–1707.

Merlivat L., Leiu M., Neif G. and Roth E. (1976) Spallation deuterium in rock 70215. In *Proc. 7th Lunar Sci. Conf.*, pp. 649–658.

Métrich N., Wallace P. J., Putirka K. D., Tepley F. J. (2008) Volatile abundances in basaltic magmas and their degassing paths tracked by melt inclusions. In Minerals, Inclusions and Volcanic Processes. Rev. Mineral. Geochem., vol. 69. Mineralogical Society of America and Geochemical Society, pp. 365–402.

Meyer, C., 2009. Lunar sample compendium

Moore L. R., Gazel E., Tuohy R., Lloyd A. S., Esposito R., Steele-MacInnis M., Hauri E. H., Wallace P. J., Plank T. and Bodnar R. J. (2015) Bubbles matter: An assessment of the contribution of vapor bubbles to melt inclusion volatile budgets. *Am. Mineral.* **100**, 806–823.

Mosenfelder J. L., Le Voyer M., Rossman G. R., Guan Y., Bell D. R., Asimow P. D. and Eiler J. M. (2011) Analysis of hydrogen in olivine by SIMS: evaluation of standards and protocol. *Am. Mineral.* **96**, 1725–1741.

Moynier F., Albarède F. and Herzog G. F. (2006) Isotopic composition of zinc, copper, and iron in lunar samples. *Geochim. Cosmochim. Acta* **70**, 6103–6117.

Nemchin A. A., Timms N., Pidgeon R., Geisler T., Reddy S. and Meyer C. (2009) Timing of crystallization of the lunar magma ocean constrained by the oldest zircon. *Nat. Geosci.* **2**, 133–136.

Newman S., Epstein S. and Stolper E. (1988) Water, carbon dioxide, and hydrogen isotopes in glasses from the ca.1340 A.D. eruption of the Mono craters, California: constraints on degassing phenomena and initial volatile content. *J. Volcanol. Geotherm. Res.* **35**, 75–96.

Newton R. C., Anderson A. T. and Smith J. V. (1971) Accumulation of olivine in rock 12040 and other basaltic fragments in the light of analysis and syntheses. In *Proc. Second Lunar Sci. Conf.*, pp. 575–582.

Ni P., Zhang Y. and Guan Y. (2017) Volatile loss during homogenization of lunar melt inclusions. *Earth Planet. Sci. Lett.* **478**, 214–224.

Ni P., Zhang Y., Chen S. and Gagnon J. (2019) A melt inclusion study on volatile abundances in the lunar mantle. *Geochim. Cosmochim. Acta* **249**, 17–41.

Nowak M. and Behrens H. (1995) The speciation of water in haplogranitic glasses and melts determined by in situ nearinfrared spectroscopy. *Geochim. Cosmochim. Acta* **59**(16), 3445–3450.

Pahlevan K. and Stevenson D. J. (2007) Equilibration in the aftermath of the lunar-forming giant impact. *Earth Planet. Sci. Lett.* **262**, 438–449.

Palme H. and O'Neil H. S. C. (2014) Cosmochemical estimates of mantle composition. *Treatise Geochem.*, 1–39.

Paniello R. C., Day J. M. D. and Moynier F. (2012) Zinc isotopic evidence for the origin of the Moon. *Nature* **490**, 376–379.

Peslier A. H., Schönbächler M. and Busemann H. (2017) Water in the Earth's interior: distribution and origin. *Space Sci. Rev.* **212**, 743–811.

Peslier A. H., Hervig R., Yang S., Humayun M., Barnes J. J., Irving A. J. and Brandon A. D. (2019) Determination of the water content and D/H ratio of the martian mantle y unravelling degassing and crystallisation effects in nakhlites. *Geochim. Cosmochim. Acta* **266**, 382–415.

Pineau F., Shilobreeva S., Kadik A. and Javoy M. (1998) Water solubility and D/H fractionation in the system basaltic andesite–H2O at 1250 °C and between 0.5 and 3 kbars. *Chem. Geol.* **147**, 173–184.

Portnyagin M., Almeev R., Matveev S. and Holtz F. (2008) Experimental evidence for rapid water exchange between melt inclusions in olivine and host magma. *Earth Planet. Sci. Lett.* **272**, 541–552.

Potts N., Barnes J. J., Tartèse R., Franchi I. A. and Anand M. (2018) Chlorine isotopic compositions of apatite in Apollo 14 rocks: evidence for widespread vapor-phase metasomatism on the lunar nearside ~4billion years ago. *Geochim. Cosmochim. Acta* **230**, 46–59.

Pringle E. and Moynier F. (2017) Rubidium isotopic composition of the Earth, meteorites, and the Moon: evidence for the origin of volatile loss during planetary accretion. *Earth Planet. Sci. Lett.* **473**, 62–70.

Renggli C. J., King P. L., Henley R. W. and Norman M. D. (2017) Volcanic gas composition, metal dispersion and deposition during explosive volcanic eruptions on the Moon. *Geochim. Cosmochim. Acta* **206**, 296–311.

Riciputi L. R. and Greenwood J. P. (1998) Analysis of sulfur and carbon isotope ratios in mixed matrices by SIMS: implications for mass bias corrections. *Int. J. Mass Spectrom. Ion Process.* **178**, 65–71.

Robinson K. L., Barnes J. J., Nagashima K., Thomen A. and Franchi I. A., et al. (2016) Water in evolved lunar rocks: evidence for multiple reservoirs. *Geochim. Cosmochim. Acta* **188**, 244–260.

Robinson K. L. and Taylor G. J. (2014) Heterogeneous distribution of water in the Moon. *Nat. Geosci.* **7**, 401–408.

Rhodes J. M. and Blanchard D. P. (1980) Chemistry of Apollo 11 low-K mare basalts. In *Proc. 11th Lunar Planet. Sci. Conf*, pp. 49–66.

Rhodes J. M., Blanchard D. P., Dungan M. A., Brannon J. C. and Rodgers K. V. (1977) Chemistry of Apollo 12 mare basalts: magma types and fractionation processes. In *Proc. 8th Lunar Sci. Conf.*, pp. 1305–1338.

Rhodes J. M. and Hubbard N. J. (1973) Chemistry, classification and petrogenesis of Apollo 15 mare basalts. In *Proc. 4th Lunar Sci. Conf.*, pp. 1127–1148.

Roedder E. and Weiblen P. W. (1970) Lunar petrology of silicate melt inclusions, Apollo 11 rocks. In Proceedings of the Apollo 11 Lunar Science Conference, vol.1, pp.801–837.

Roedder E. and Weiblen P. W. (1971) Petrology of silicate melt inclusions, Apollo 11 and Apollo 12 and terrestrial equivalents. In Proceedings of the Second Lunar Science Conference, vol.1, pp. 507–528.

Roedder E. (1979) Origin and significance of magmatic inclusions. *Bull. Mineral.* **102**, 487–510.

Roedder E. (1984) Occurrence and significance of magmatic inclusions and silicate liquid immiscibility. *Acta Geol. Pol.* **34** (1–2), 139–178.

Roskosz M., Deloule E., Ingrin J., Depecker C., Laporte D., Merkel S., Remusat L. and Leroux H. (2018) Kinetic D/H fractionation during hydration and dehydration of silicate glasses, melts and nominally anhydrous minerals. *Geochim. Cosmochim. Acta* **233**, 14–32.

Rumpf M. E. et al. (2013). *JGR- Planets* **118**, 382–397.

Saal A. E. et al. (2008) Volatile content of lunar volcanic glasses and the presence of water in the Moon's interior. *Nature* **454**, 192–195.

Saal A. E., Hauri E. H., Van Orman J. A. and Rutherford M. J. (2013) Hydrogen isotopes in lunar volcanic glasses and melt inclusions reveal a carbonaceous chondrite heritage. *Science* **340**, 1317–1320.

Severs M. J., Azbej T., Thomas J. B., Mandeville C. W. and Bodnar R. J. (2007) Experimental determination of $H_2O$ loss from melt inclusions during laboratory heating: Evidence from Raman spectroscopy. *Chem. Geol.* **237**, 358–371.

Sharp Z. D., Shearer C. K., McKeegan K. D., Barnes J. D. and Wang Y. Q. (2010) The chlorine isotope composition of the Moon and implications for an anhydrous mantle. *Science* **329**, 1050–1053.

Shaw A. M., Hauri E. H., Fischer T. P., Hilton D. R. and Kelley K. A. (2008) Hydrogen isotopes in Mariana arc melt inclusions: implications for subduction dehydration and the deep-Earth water cycle. *Earth Planet. Sci. Lett.* **275**, 138–145.

Sharp Z. D., McCubbin F. M. and Shearer C. K. (2013) A hydrogen-based oxidation mechanism relevant to planetary formation. *Earth and Planetary Science Letters* **380**, 88–97.

Shearer C. K. and Papike J. J. (1993) Basaltic magmatism on the Moon: a perspective from volcanic picritic glass beads. *Geochim. Cosmochim. Acta* **57**(19), 4785–4812. https://doi.org/10.1016/0016-7037(93)90200-G.

Singer J. A., Greenwood J. P., Itoh S., Sakamoto N. and Yurimoto H. (2017) Evidence for the solar wind in lunar magmas: A study of slowly cooled samples of the Apollo 12 olivine basalt suite. *Geochem. J.* **51**, 95–104.

Snape J. F., Nemchin A. A., Bellucci J. J., Whitehouse M. J., Tartèse R., Barnes J. J., Anand M., Crawford I. A. and Joy K. H. (2016) Lunar basalt chronology, mantle differentiation and implications for determining the age of the Moon. *Earth Planet. Sci. Lett.* **451**, 149–158.

Steele-MacInnis M., Esposito R. and Bodnar R. J. (2011) Thermodynamic model for the effect of post-entrapment crystallization on the H2O-CO2 systematics of vapor-saturated, silicate melt inclusions. *J. Petrol.* **52**(12), 2461–2482.

Stephant A. and Robert F. (2014). The negligible chondritic contribution to lunar soils water. Proc. Natl. Am. Soc 111 (42), 15007–15012.

Stephant A., Anand M., Zhao X., Chan Q. H. S. E., Bonifacie M. and Franchi I. A. (2019) The chlorine isotopic composition of the Moon: Insights from melt inclusions. *Earth Planet. Sci. Lett.* **553** 115715.

Stettler A., Peter Eberhard, Geiss J., Grogler N. and Maurer P. (1973) Ar39-Ar40 ages and Ar37-Ar38 exposure ages of lunar rocks. In *Proc. 4th Lunar Sci. Conf.*, pp. 1865–1888.

Tartèse R. and Anand M. (2013) Late delivery of chondritic hydrogen into the lunar mantle: insights from mare basalts. *Earth Planet. Sci. Lett.* **361**, 480–486.

Tartèse R. et al. (2013) The abundance, distribution, and isotopic composition of hydrogen in the Moon as revealed by basaltic lunar samples: implications for the volatile inventory of the Moon. *Geochim. Cosmochim. Acta* **122**, 58–74.

Tartèse R. et al. (2014) Apatites in lunar KREEP basalts: the missing link to understanding the H isotope systematics of the Moon. *Geology* **42**, 363–366.

Taylor S. R., Kaye M., Muir P., Nance W., Rudowski R. and Ware N. (1972) Composition of the lunar uplands: chemistry of Apollo 14 samples from Fra Mauro. In *Proc. 3rd Lunar Sci. Conf.*, pp. 1231–1249.

Taylor L. A., Patchen A., Mayne R. G. and Taylor D.-H. (2004) The most reduced rock from the Moon, Apollo 14 basalt 14053: its unique features and their origin. *Am. Mineral.* **89**, 1617–1624.

Taylor S. R. (2014) The Moon re-examined. *Geochim. Cosmochim. Acta* **141**, 670–676.

Tenner T. J., Hirschmann M. M., Withers A. C. and Hervig R. L. (2009) Hydrogen partitioning between nominally anhydrous upper mantle minerals and melt between 3 and 5 GPa and applications to hydrous peridotite partial melting. *Chem. Geol.* **262**, 42–56.

Tikoo S. M., Weiss B. P., Buz J., Lima E. A., Shea E. K., Melo G. and Grove T. L. (2012) Magnetic fidelity of lunar samples and implications for an ancient core dynamo. *Earth Planet. Sci. Lett.* **337–338**, 93–103.

Treiman A. H., Boyce J. W., Gross J., Guan Y., Eiler J. M. and Stolper E. M. (2014) Phosphate-halogen metasomatism of lunar granulite 79215: impact-induced fractionation of volatiles and incompatible elements. *Am. Mineral.* **99**, 1860–1870.

Treiman A. H., Boyce J. W., Greenwood J. P., Eiler J. M., Gross J., Guan Y., Ma C. and Stolper E. M. (2016) D-poor hydrogen in lunar mare basalts assimilated from lunar regolith. *Am. Mineral.* **101**(7), 1596–1603.

Usui T., Alexander C. M. O'D., Wang J., Simon J. I. and Jones J. H. (2012) Origin of water and mantle-crust interactions on Mars inferred from hydrogen isotopes and volatile element abundances of olivine-hosted melt inclusions of primitive shergottites. *Earth Planet. Sci. Lett.* **357–358**, 119–129.

Wallace P. J. (2005) Volatiles in subduction zone magmas: concentrations and fluxes based on melt inclusion and volcanic gas data. *J. Volcanol. Geotherm. Res.* **140**, 217–240.

Walker D., Longhi J., Kirkpatrick R. J. and Hays J. F. (1976) Differentiation of an Apollo 12 pricrite magma. In *Proceedings of the 7th Lunar Science Conference*, pp. 1365–1389.

Wang K. and Jacobsen S. B. (2016) Potassium isotopic evidence for a high-energy giant impact origin of the Moon. *Nature* **538**, 487–490.

Wang Y., Hsu W. and Guan Y. (2019) An extremely heavy chlorine reservoir in the Moon: Insights from the apatite in lunar meteorites. *Sci. Rep.* **9**, 5727.

Wiens R. C., Bochsler P., Burnett D. S. and Wimmer-Schweingruber R. F. (2004) Solar and solar wind isotopic compositions. *Earth and Planetary Science Letters* **226**, 549–565.

Willis J. P., Ahrens L. H., Danchin R. V., Erlank A. J., Gurney J. J., Hofmeyr P. K., McCarthy T. S. and Orren M. J. (1971) Some inter-element relationships between lunar rocks and fines, and stony meteorites. In *Proc. Lunar Sci. Conf.*, pp. 1123–1138.

Yaxley G. M., KamenetskyV S., Kamenetshy M., Norman M. D. and Francis D. (2004) Origins of compositional heterogeneity in olivine-hosted melt inclusions from the Baffin Island picrites. *Contributions to Mineralogy and Petrology* **148**, 426–442.

York D., Kenyon W. J. and Doyle R. J. (1972) 40Ar-39Ar ages of Apollo 14 and 15 samples. In *Proc. 3rd Lunar Sci. Conf.*, pp. 1613–1622.

Zhang Y. (2014) Degassing history of Earth. In *Treatise on Geochemistry* (eds. H. D. Holland and K. K. Turekian), 2nd ed. Elsevier, Oxford, pp. 37–69.

*Associate editor:* Marc Norman